The last months in a nutshell

APHE Meeting, 4th July 2024

Calibration of the flat-field flasher

by Maëlle Perois

&

Stellar Intensity Interferometry

Medium Size Telescope + NectarCAM

Credits: CTAO

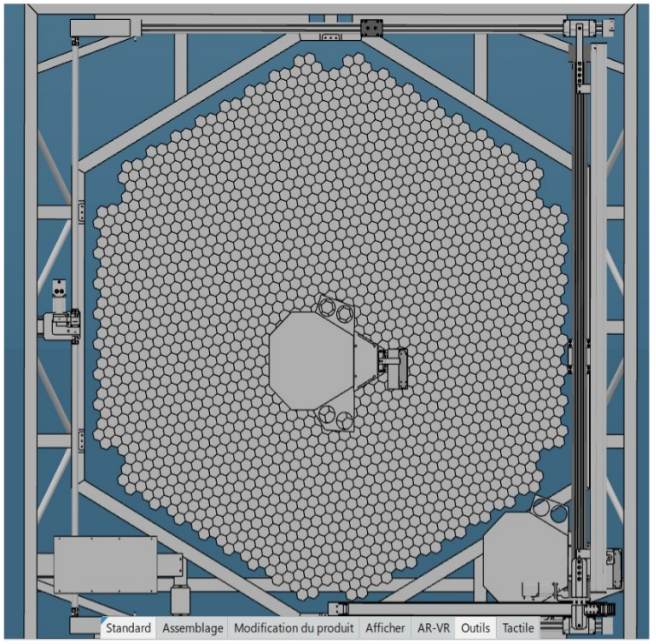

Credits: K. Pressard (IJCLab)

Dark room setup

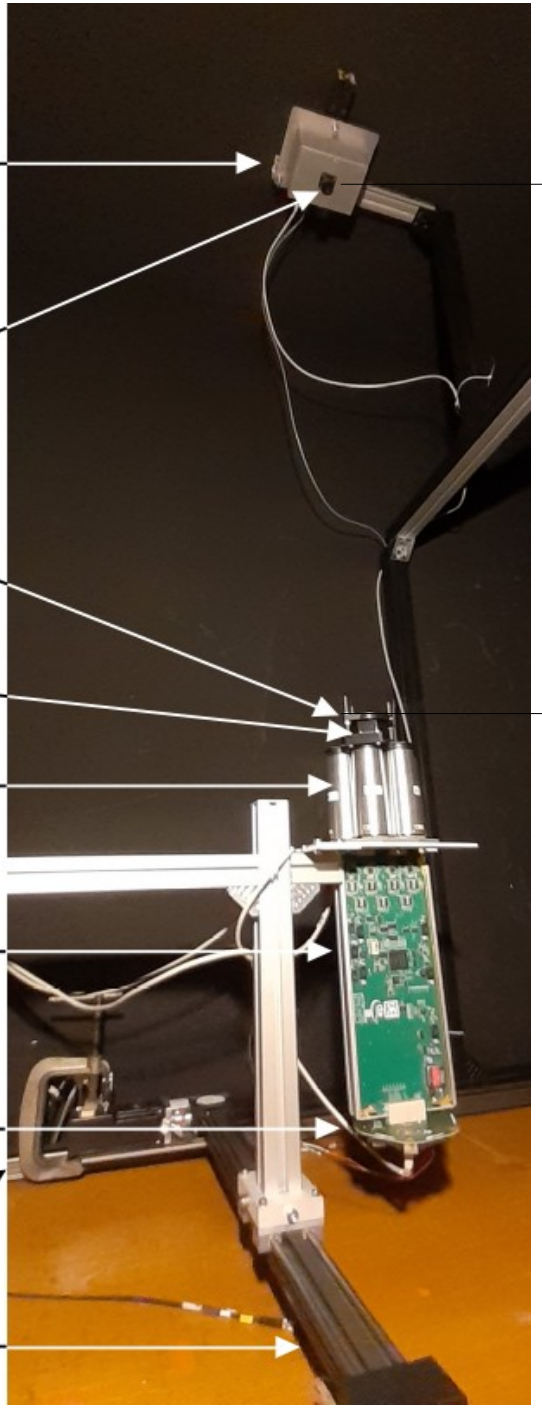

Caractérisation de la réponse angulaire du pulseur de lumière à champ plat pour la caméra NectarCAM

Maëlle Perois, A2C/APHE

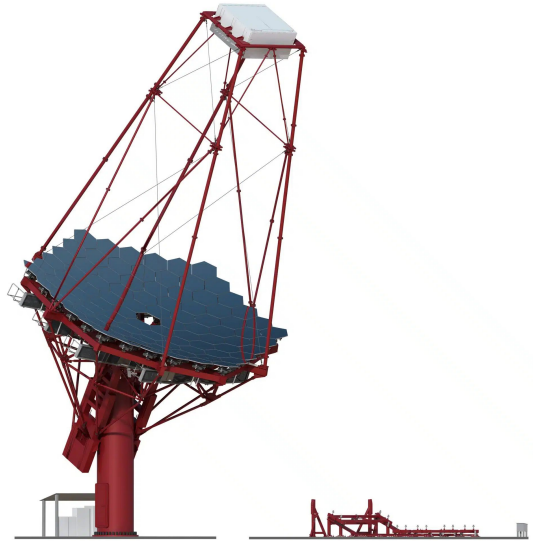

MST Rendering (Credit: Gabriel Pérez Díaz, IAC)

Encadrants : Jonathan Biteau, Quentin Luce

Presentation of the set up

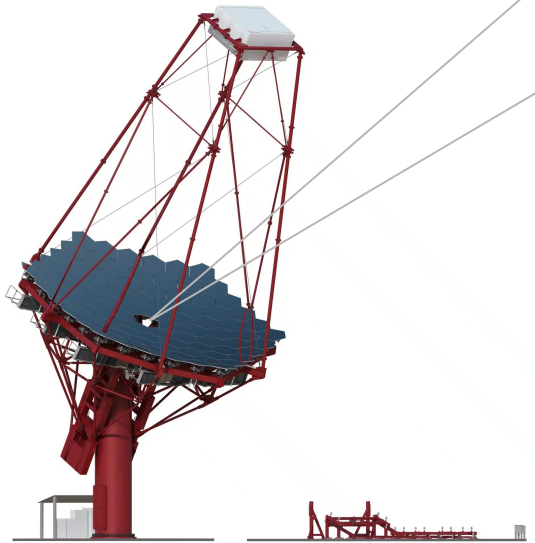

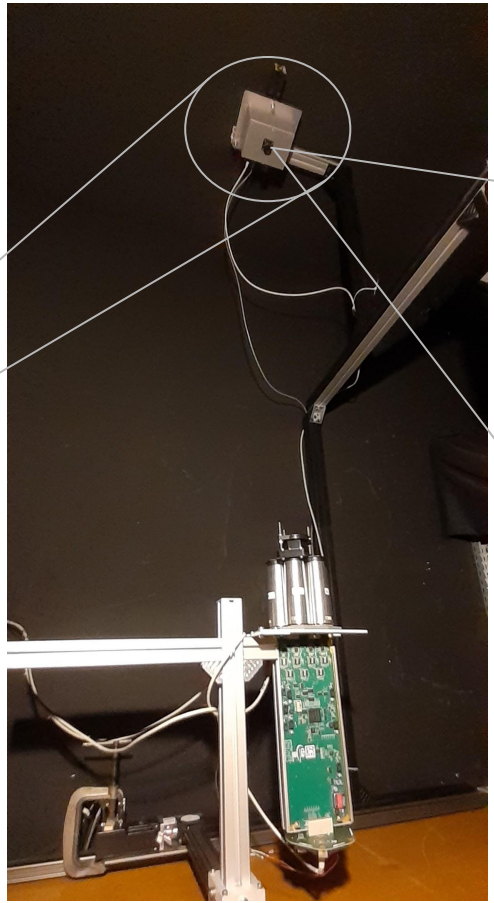

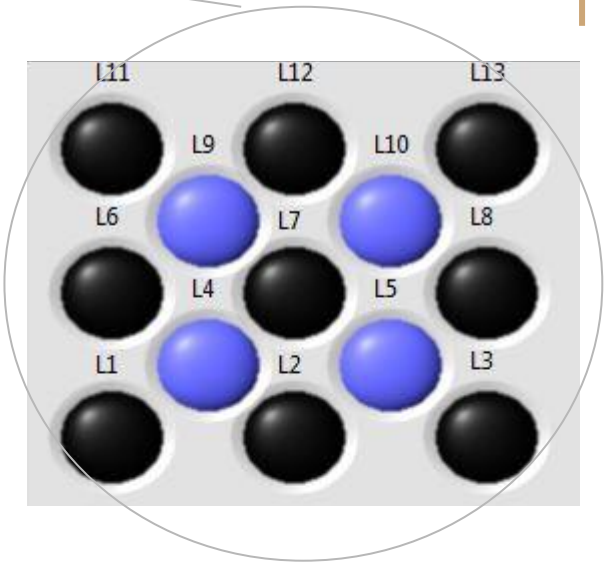

Light intensity measurement for one LED configuration

Example of a pair low gain / high gain of histograms of light intensity, for a position (X,Y) for the LED configuration “small square” (L4L5L9L10)

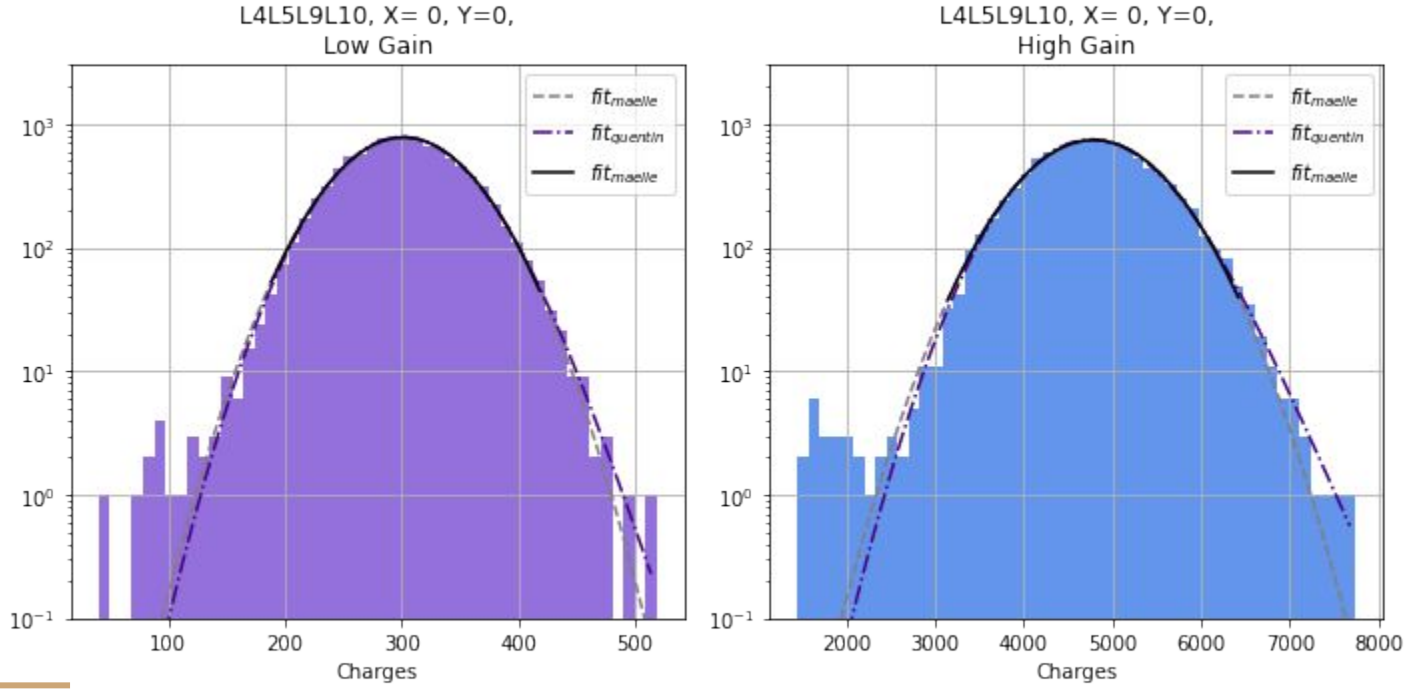

Light intensity measurement for one LED configuration

Heat map of the measured light intensity as a function of the position

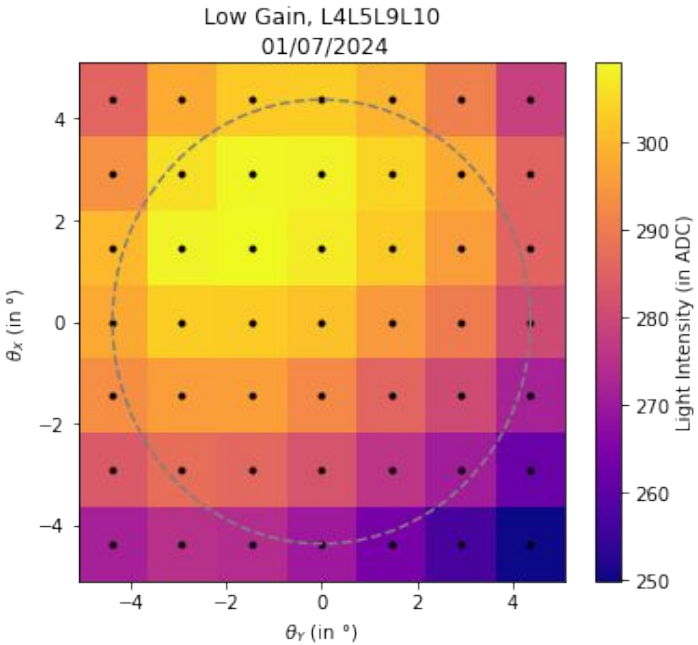

Heat map of the light intensity fitted as a function of the position

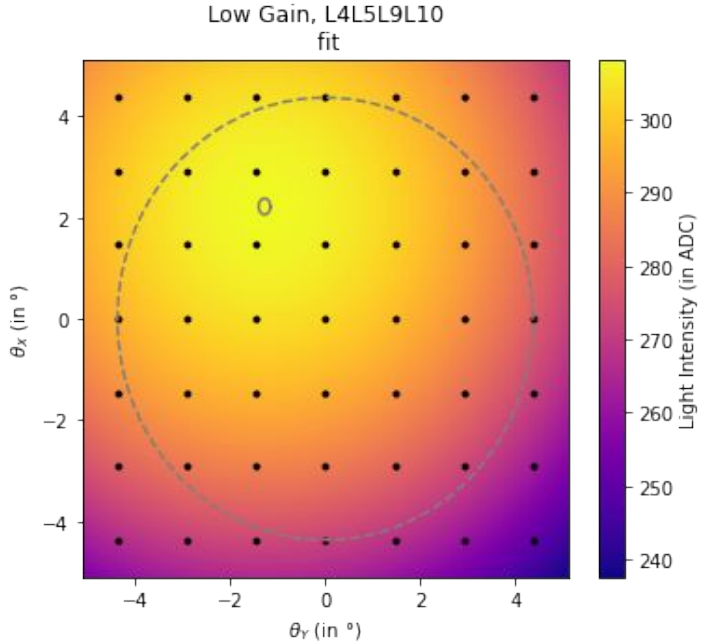

Evolution of normalised residuals

Normalised residuals between measurements and the fitted model depending on the position (X,Y) for the LED configuration “small square” (L4L5L9L10)

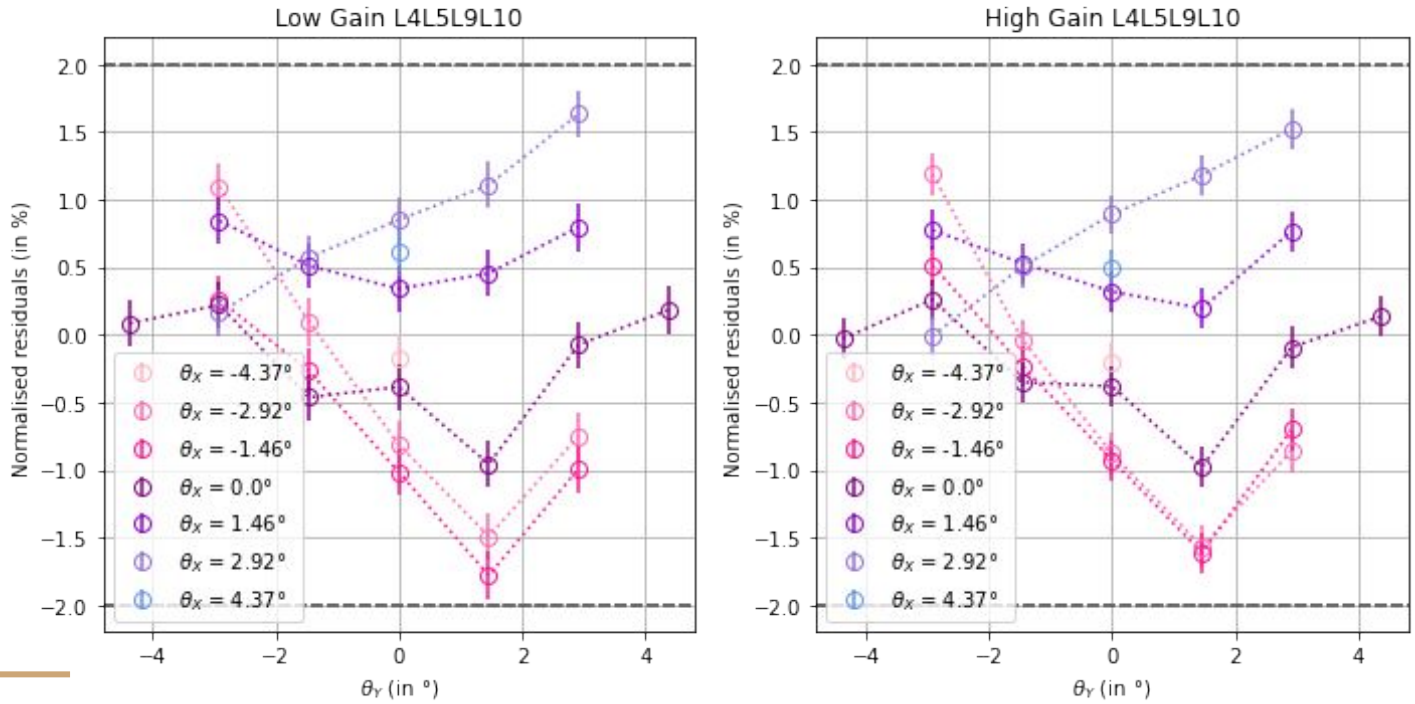

Conclusion

what has been done :

- ★ development of the experimental protocol to calibrate the flat-field flasher
- ★ measurements made for 3 LED configurations with two different focal plane module
- ★ construction and fit of the first light intensity maps

what is need to be done :

- ★ more precise alignment of the set up
- ★ measurements for the 3 LED configurations with the new focal plane module and reconstruction of the light intensity map
- ★ check if the previous models can be applied to the new measurements : are the normalised residuals under 2% ?

Back up slides

Temperature analysis

Temperature evolution of the differents electronic components as a function of the time

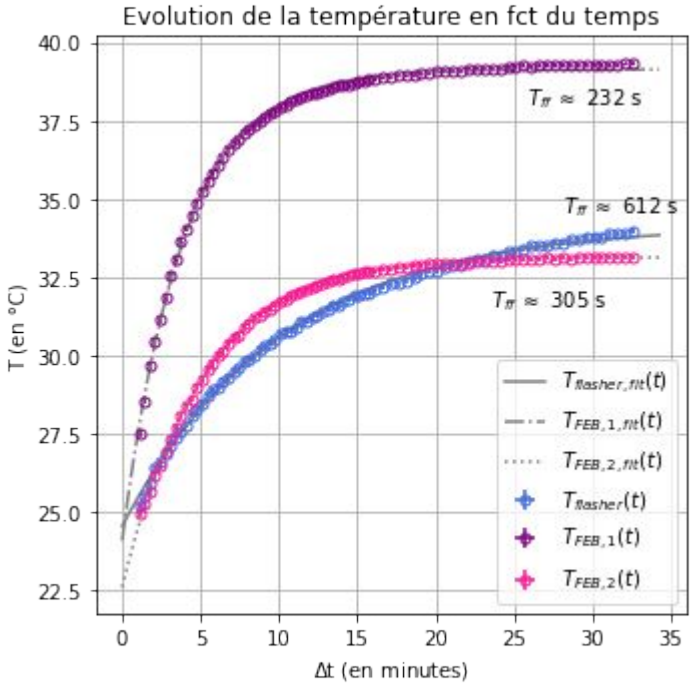

Light intensity measurement for one LED configuration

Heat map of the measured light intensity as a function of the position

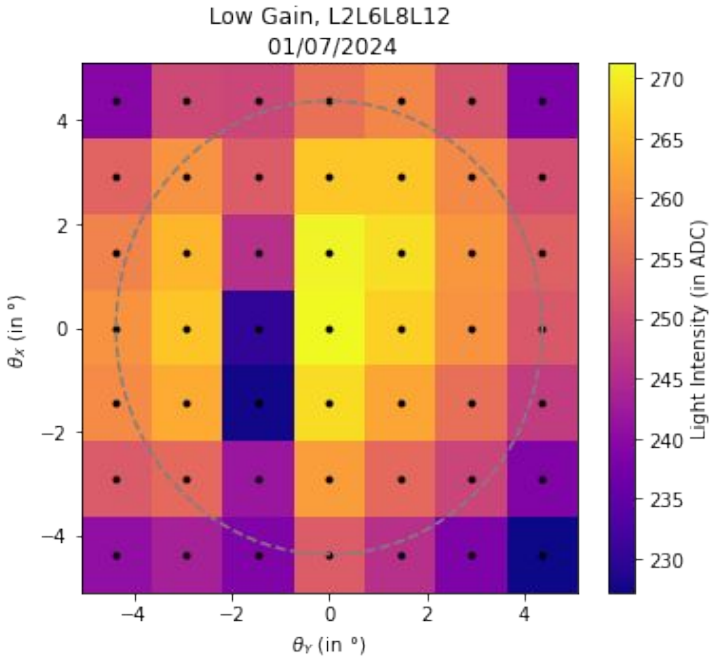

Heat map of the light intensity fitted as a function of the position

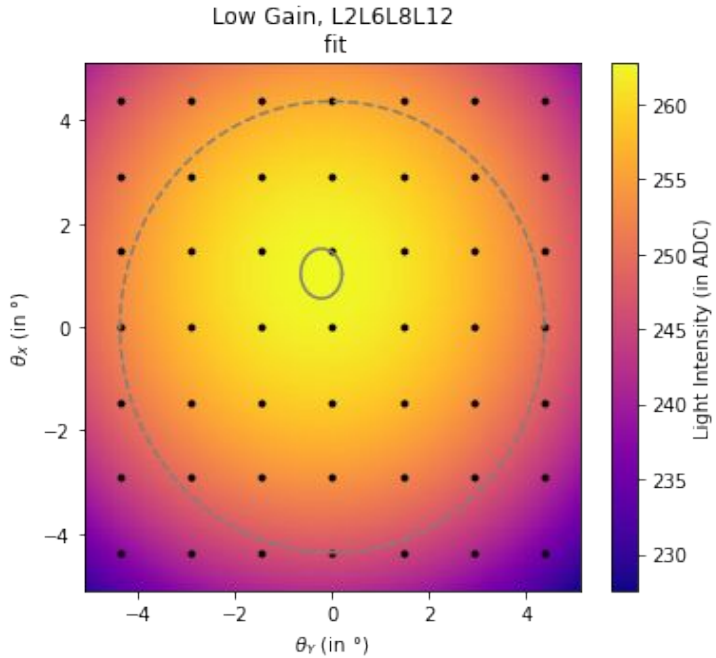

Evolution of normalised residuals

Normalised residuals between measurements and the fitted model depending on the position (X,Y) for the LED configuration “small square” (L2L6L8L12)

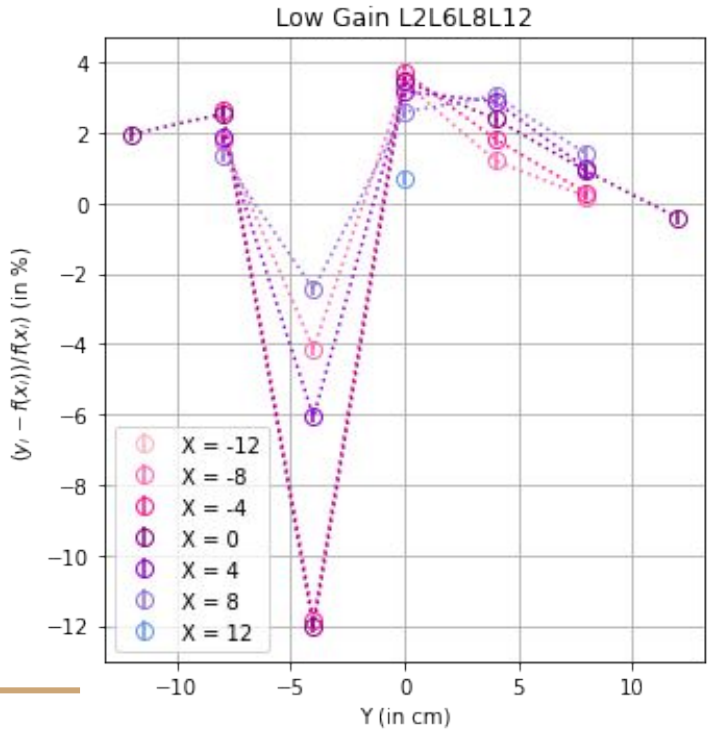

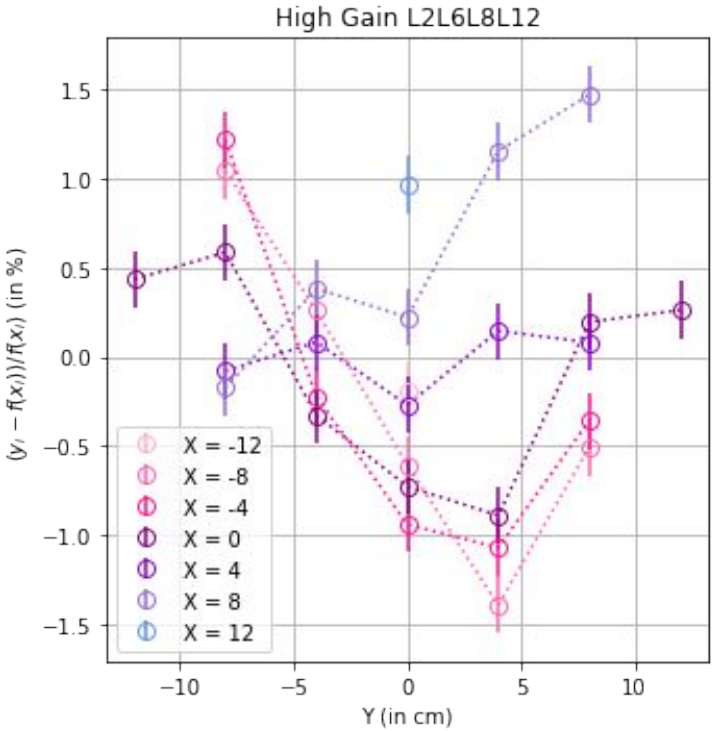

Stellar Intensity Interferometry

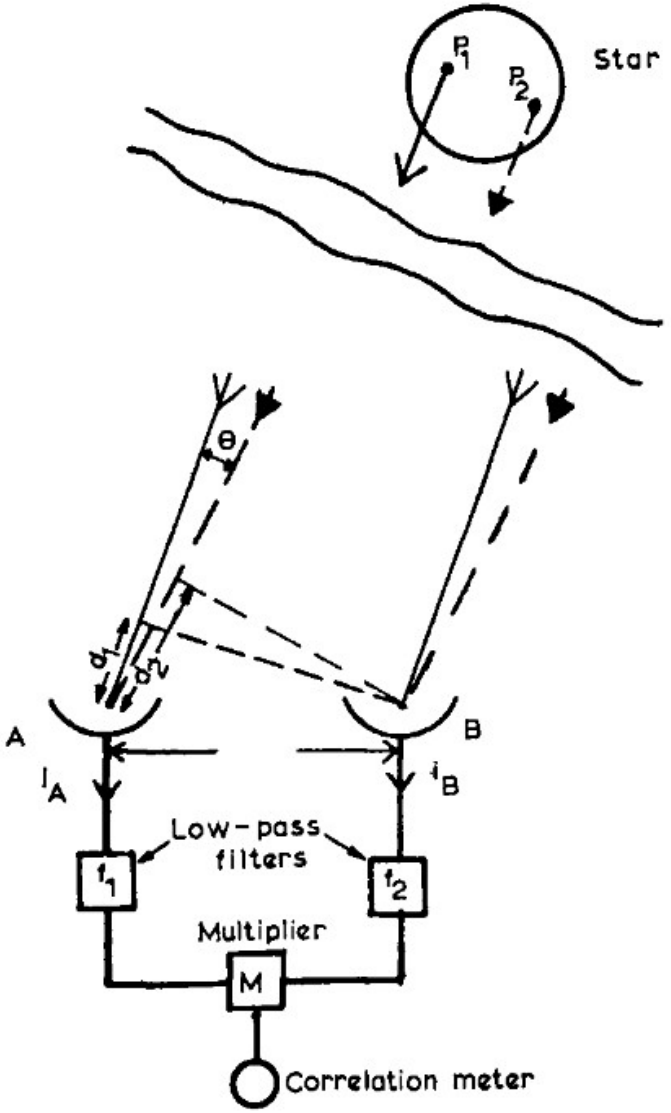

Fig. 2.5. Illustrating the principle of an intensity interferometer.

SII consists in a **measurement of the spatial correlation of the intensities of the light from a star with two telescopes** at distance d (Hanbury-Brown & Twiss 1957, 1958)

$$\frac{\langle I_A I_B \rangle}{\langle I_A \rangle \langle I_B \rangle} \propto g^{(2)}(u,v,t) \propto |V|^2$$

$\langle I_A I_B \rangle$ Time averaged cross-correlation of the intensities

Digitization at each telescopes
Atmospheric inhomogeneities negligeable

Measurements of angular distances between objects or angular size with a resolution

$$\Delta\theta = \frac{\lambda}{d}$$

Hanbury-Brown (1974), book: The Intensity Interferometer

Narabri Stellar Intensity Interferometer

First intensity interferometer initiated by Hanbury-Brown and Twiss (1963 to 1974) In Narabrii (Australia)

2 mosaic reflectors with 6.5m diameter

Measurement of the **2nd order degree of coherence**

From 1963 to 1974: **measurement of the angular diameter of 32 stars**

But:
- developments in Michelson interferometry
- low signal to noise ratio

Revival with new Imaging Atmospheric Cherenkov Telescopes (baselines over km) Recent results of HESS, MAGIC and VERITAS

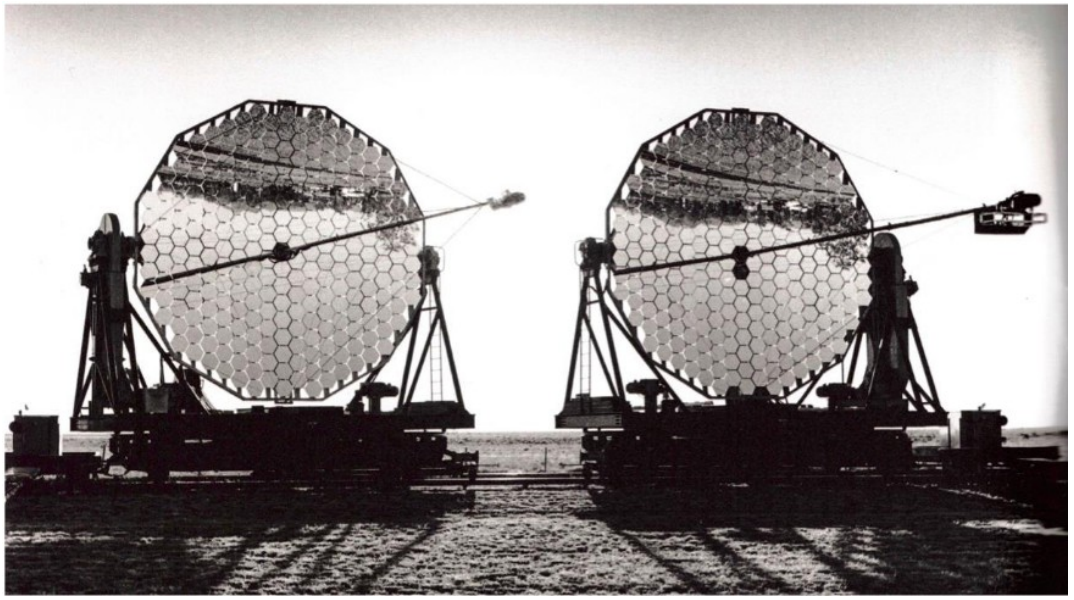

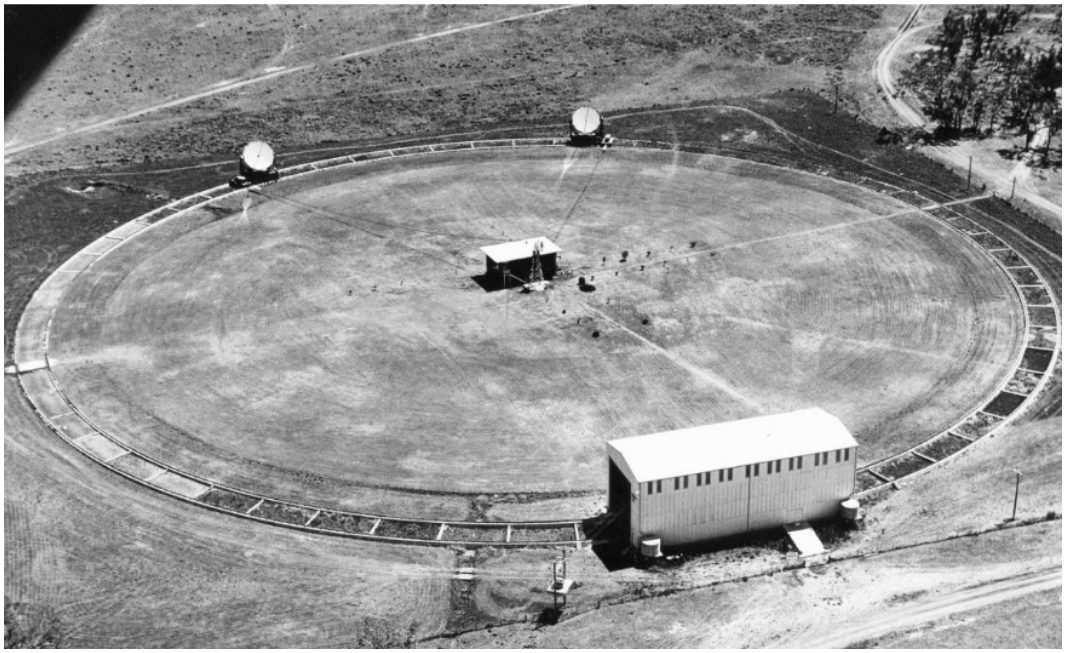

Stellar Intensity Interferometry

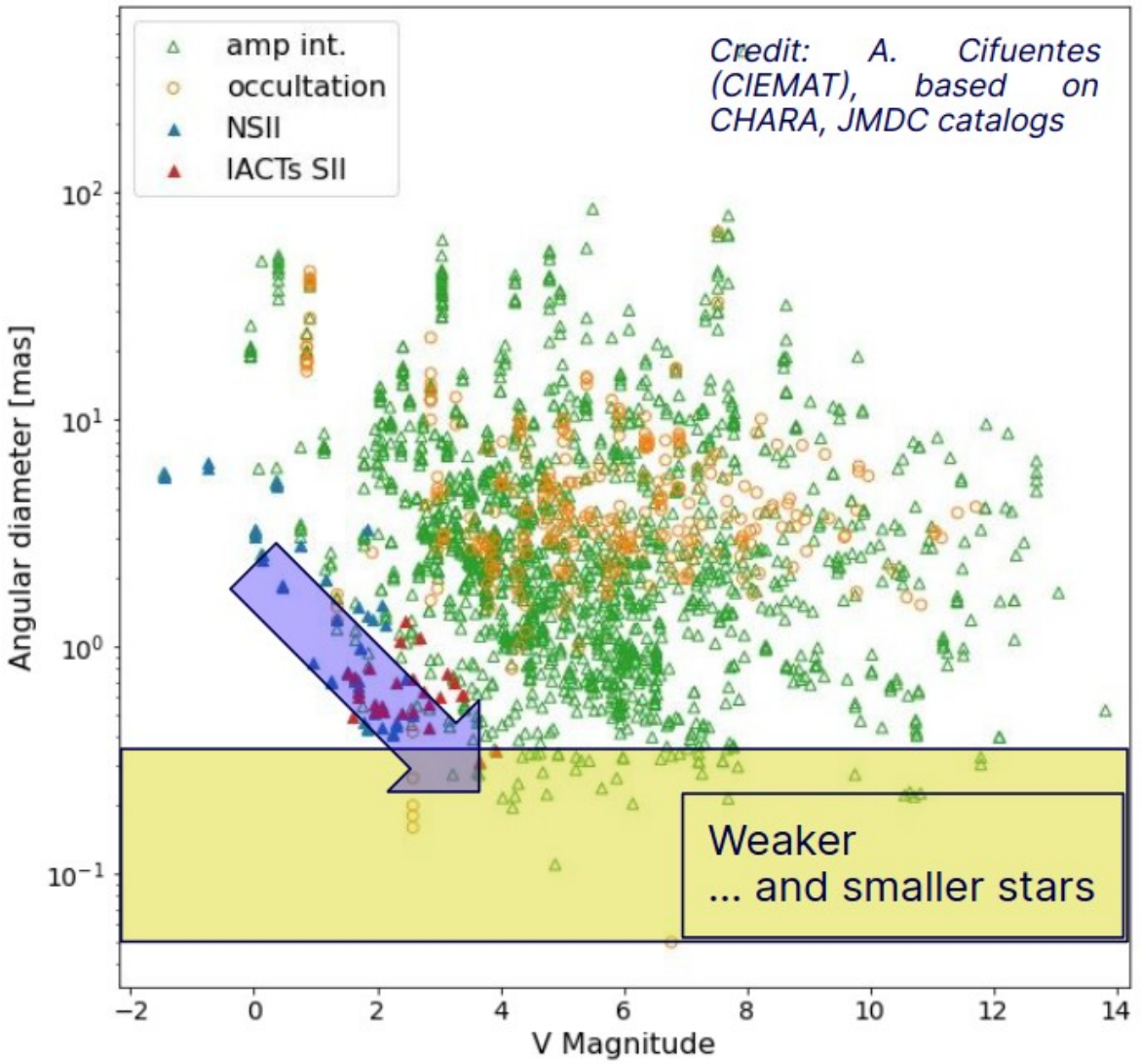

What could be observed ? sub-mas stellar diameters, oblateness/darkening in fast rotators, stellar discs/winds around massive stars, unresolved binary systems, surface features and stellar convection/magnetic activit, etc.

What do we still need for the MSTs?

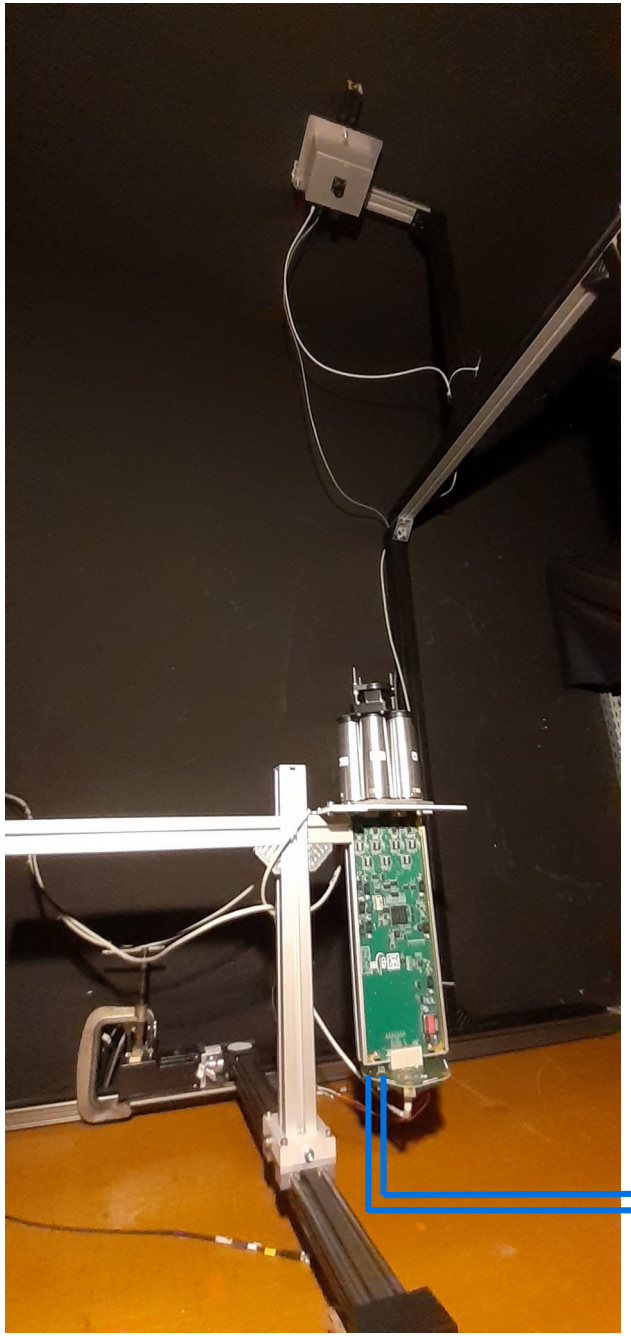

How to send the signal to the correlator?

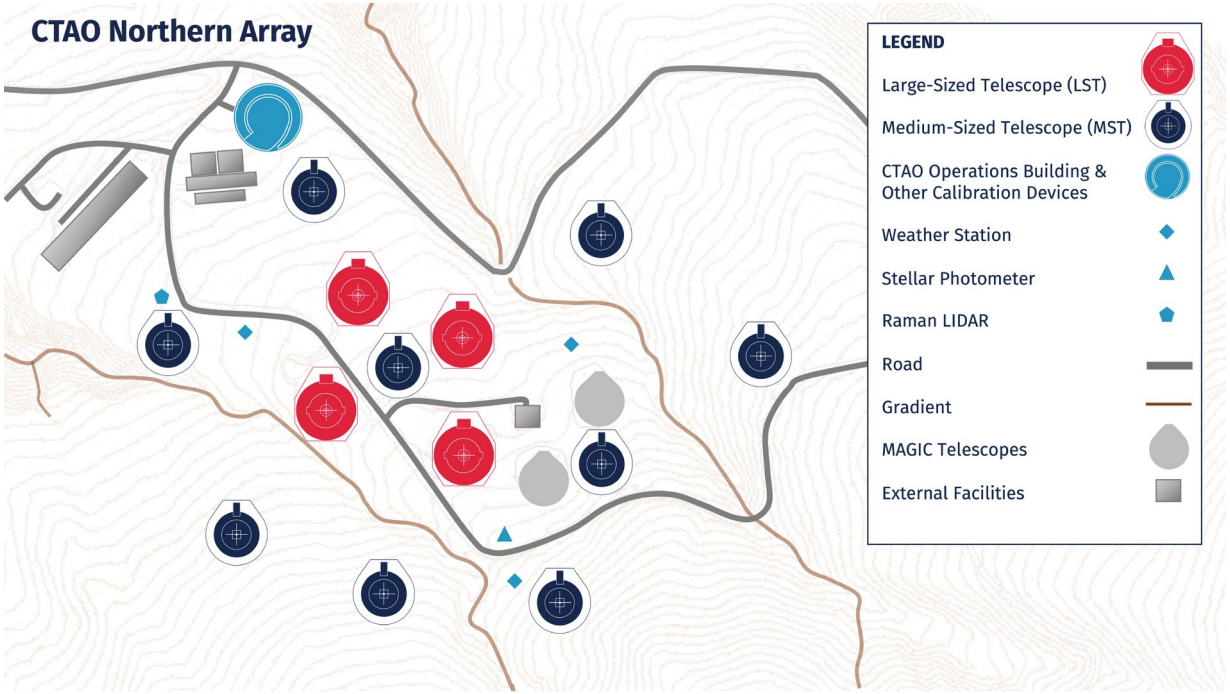

Credits: CTAO

How to extract the signal from the anode of the PMT?

Simulations of CTAO performances

$$S/N = A \cdot \alpha(\lambda_0) \cdot q(\lambda_0) \cdot n(\lambda_0) \cdot |V|^2(\lambda_0, d) \cdot \sqrt{b_\nu} \cdot F^{-1} \cdot \sqrt{T/2} \cdot (1+\beta)^{-1} \cdot \sigma$$

CTA-N	Large-Sized Telescope (LST)	Medium-Sized Telescope (MST)
	Mechanics	
Number of telescopes	4	9
Effective mirror area (including **shadowing**)	370 m²	88 m²
Primary reflector diameter	23 m	11.5 m
Focal length	28 m	16 m
Optical design	Parabolic	Modified Davies-Cotton
Arrival time standard deviation	-	0.7 ns
Pixel size (imaging)	6 arcmin	10 arcmin
95% containment diameter of point spread function In the filter plane at zenith	56 mm	33 mm
Pointing precision	< 14 arcsec	< 7 arcsec
	Optics	
Cone half angle	22 deg	20 deg
Optical efficiency at 420 nm, incl. mirror reflectivity, ~~shadowing~~, entrance window, filters, light cones	0.64	0.73
Normalized spectral distribution with a 420 nm filter, for a 21 deg cone	0.91	
	Photodetection	
PMT excess noise factor	1.21	
PMT quantum efficiency at 420 nm	39%	
PMT transit time standard deviation at 1 p.e.	1.5 ns	
	Bandwidth	
Maximum electronic bandwidth	650 MHz	600 MHz

Credits: J. Biteau (IJCLab)

Simulations of CTAO performances

$$S/N = A \cdot \alpha(\lambda_0) \cdot q(\lambda_0) \cdot n(\lambda_0) \cdot |V|^2(\lambda_0, d) \cdot \sqrt{b_\nu} \cdot F^{-1} \cdot \sqrt{T/2} \cdot (1+\beta)^{-1} \cdot \sigma$$

Example for **κ-Ori** (magnitude ~2, angular diameter ~0.4 mas, 200 min of observations):

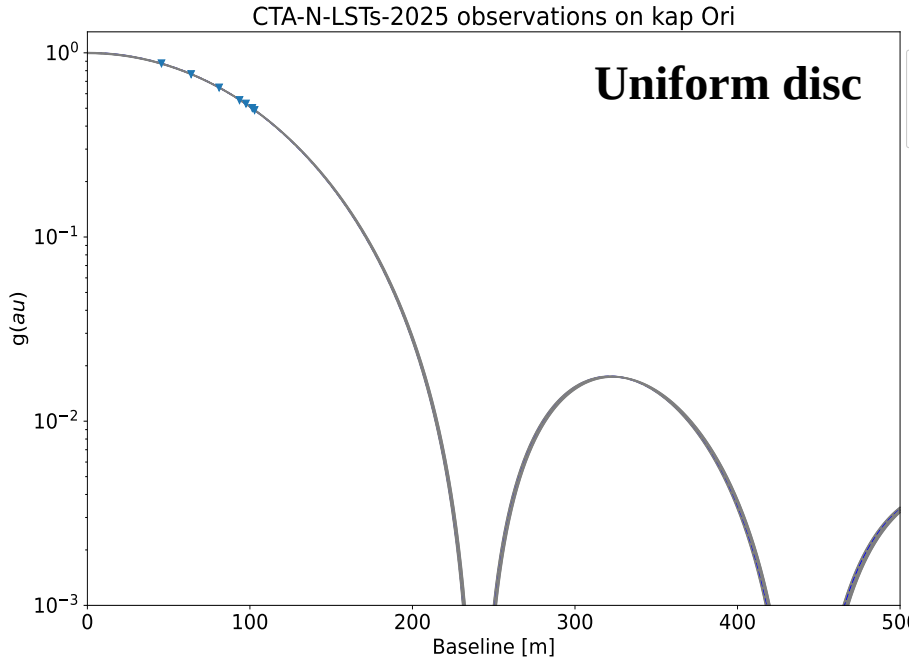

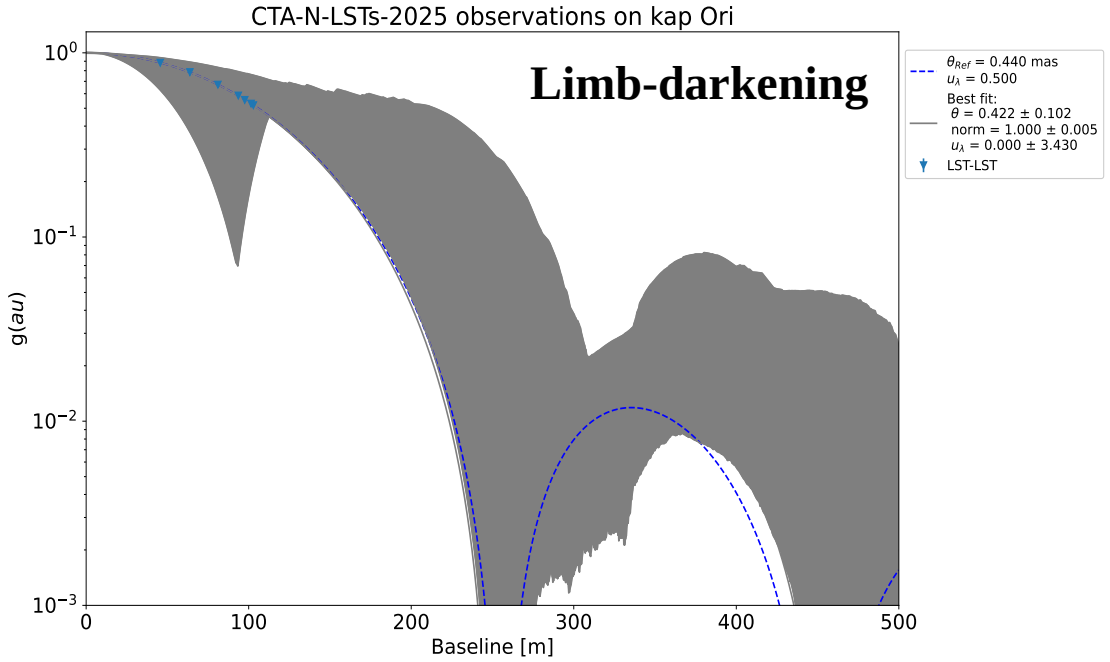

Code provided by T. Hassan (CIEMAT, Madrid)

Simulations of CTAO performances

$$S/N = A \cdot \alpha(\lambda_0) \cdot q(\lambda_0) \cdot n(\lambda_0) \cdot |V|^2(\lambda_0, d) \cdot \sqrt{b_\nu} \cdot F^{-1} \cdot \sqrt{T/2} \cdot (1+\beta)^{-1} \cdot \sigma$$

Example for **κ-Ori** (magnitude ~2, angular diameter ~0.4 mas, 200 min of observations):

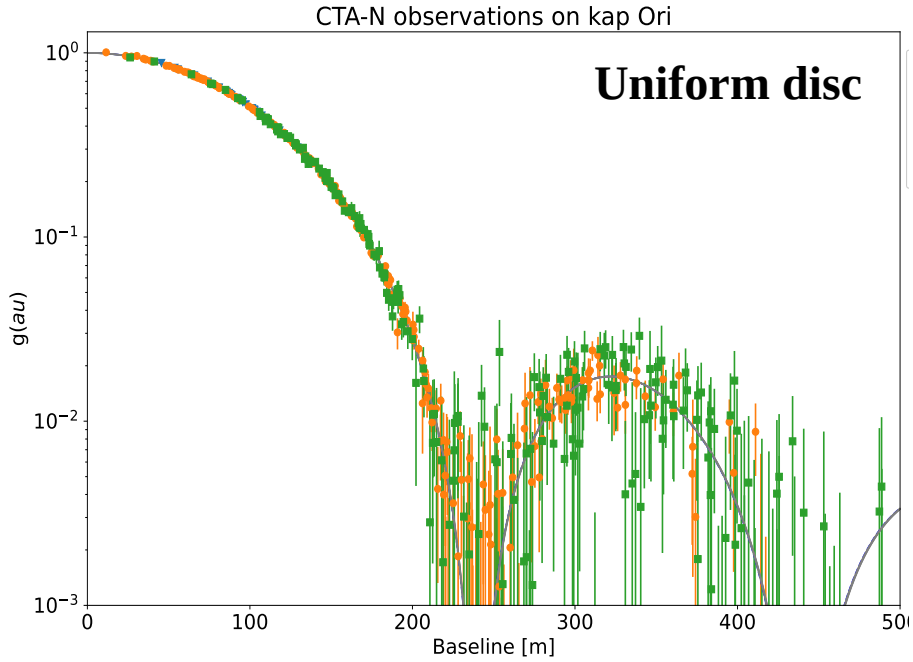

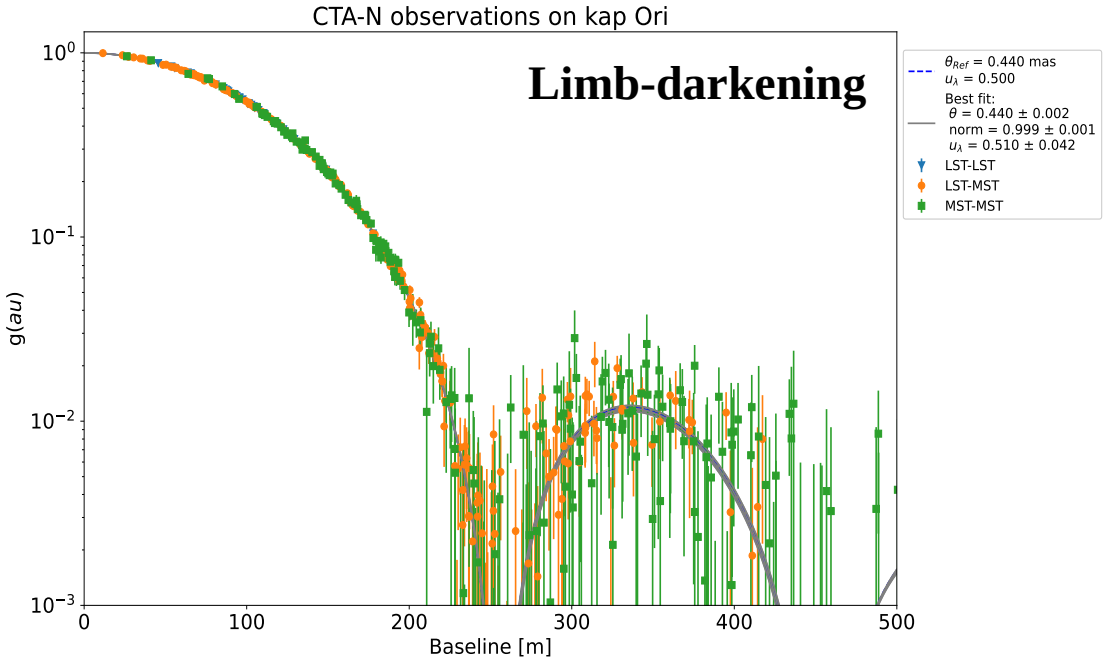

Code provided by T. Hassan (CIEMAT, Madrid)

Reachable performances?

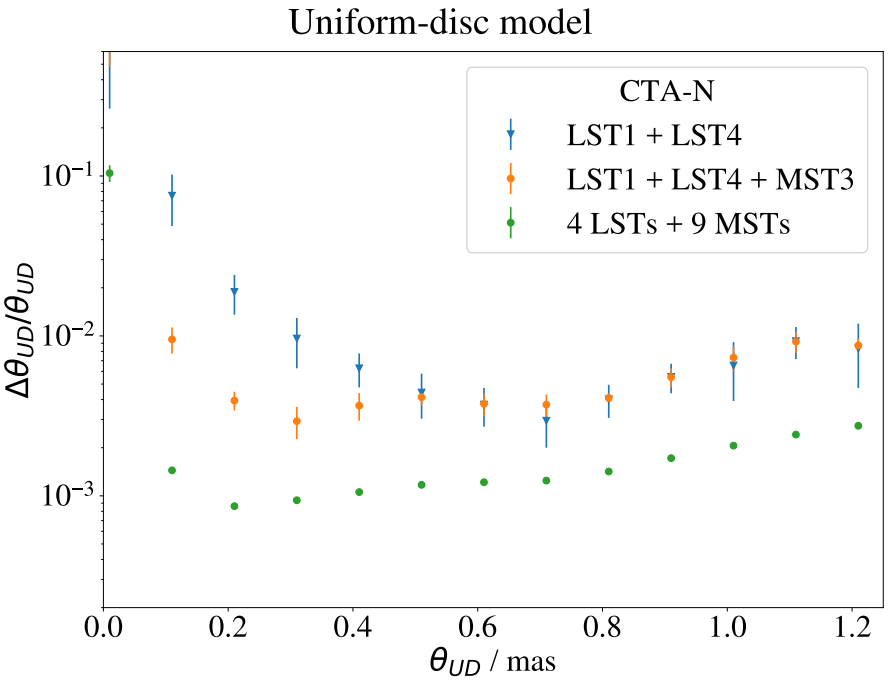

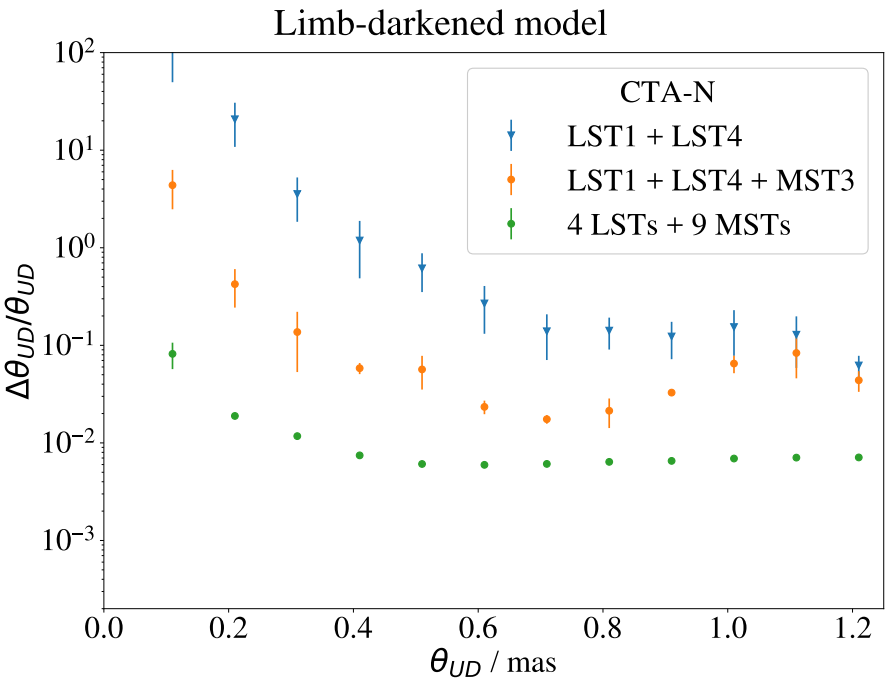

Perspectives for the next months

Simulation of a star (angular diameter, magnitude, etc.)
Uniform disk or limb-darkening

Simulation of the response of the telescopes
(Needed for the CTA data challenge)

Reconstruction of the degree of coherence
(Code from Tarek Hassan)

Imaging reconstruction
(phase model dependency, etc.?)

Perspectives for the next months

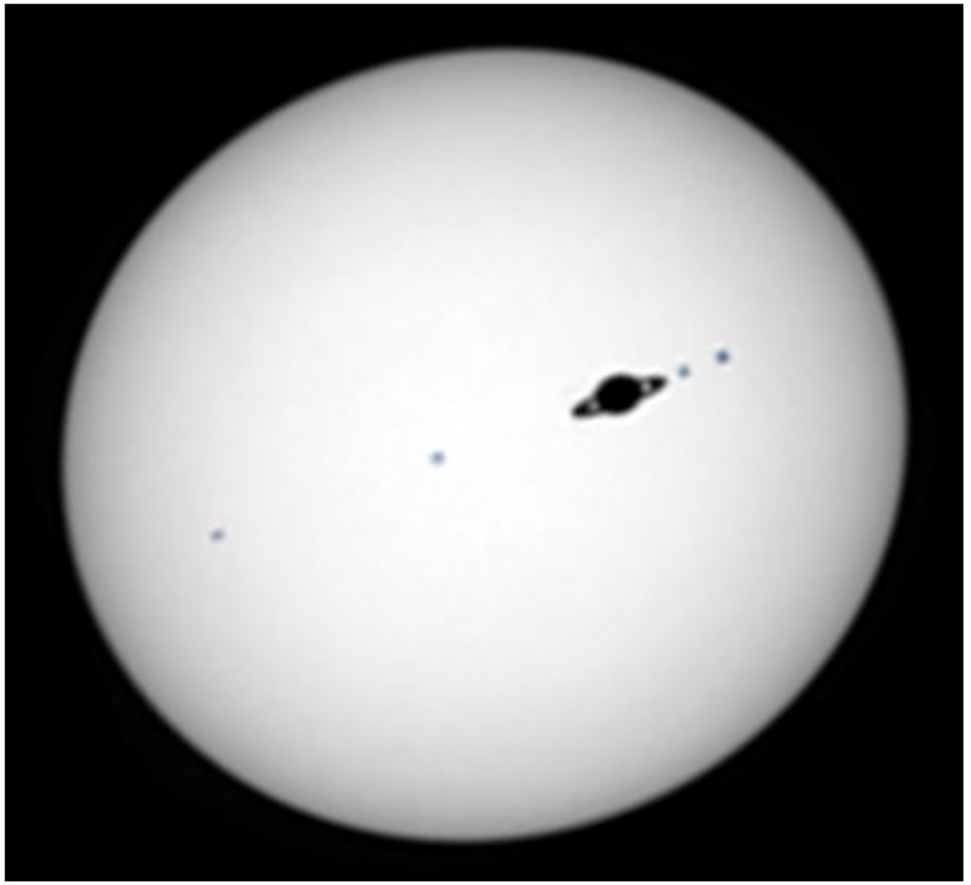

Figure 11. A vision of microarcsecond optical imaging: Expected resolution for an assumed transit of a hypothetical exoplanet across the disk of Sirius, using the Cherenkov Telescope Array as an intensity interferometer. Stellar diameter = 1.7 solar, Distance = 2.6 pc, Angular diameter = 6 mas; assumed planet of Jupiter size and oblateness; Saturn-type rings; four Earth-size moons; equatorial diameter = 350 µas. With the CTA array spanning 2 km, a 50 µas resolution provides more than 100 pixels across the stellar diameter.

Dravins et Lagadec (2014), Proc. SPIE 9146 91460Z

Back-up

A consideration of a non-identical shape of the injected spectrum within the combined fit

The combined fit recipe

From the emission rate per unit of energy:

$$\dot{Q}_{Ai}(R) = \frac{p_A(R, \gamma, R_{\max})}{R} \varepsilon_A S_i$$

Extraction of the PDF for the emitted energy E of an UHECR with mass number A:

$$p_A(R, \gamma, R_{\max}) = \frac{Rj(R, \gamma, R_{\max})}{\int_{R_{\min}}^{\infty} Rj(R, \gamma, R_{\max}) \mathrm{d}R}$$

with the injected spectrum expressed as:

$$\mathrm{j(R,}\ \gamma, R_{\max}) \propto \left(\frac{R}{R_0}\right)^{-\gamma} \begin{cases} 1 & \text{if } R < R_{\max}, \\ \exp\left(1 - \frac{R}{R_{\max}}\right) & \text{otherwise.} \end{cases}$$

Free parameters of the combined fit: $\gamma_A, \gamma_p, \lg R_{\max}, 5\ \varepsilon_A, \delta X_{\mathrm{model}}$

Data: Energy flux, X_{max}, $\sigma(X_{max})$ from the Pierre Auger Observatory

Marafico et al. (2024), to be published in ApJ

Combined fit results

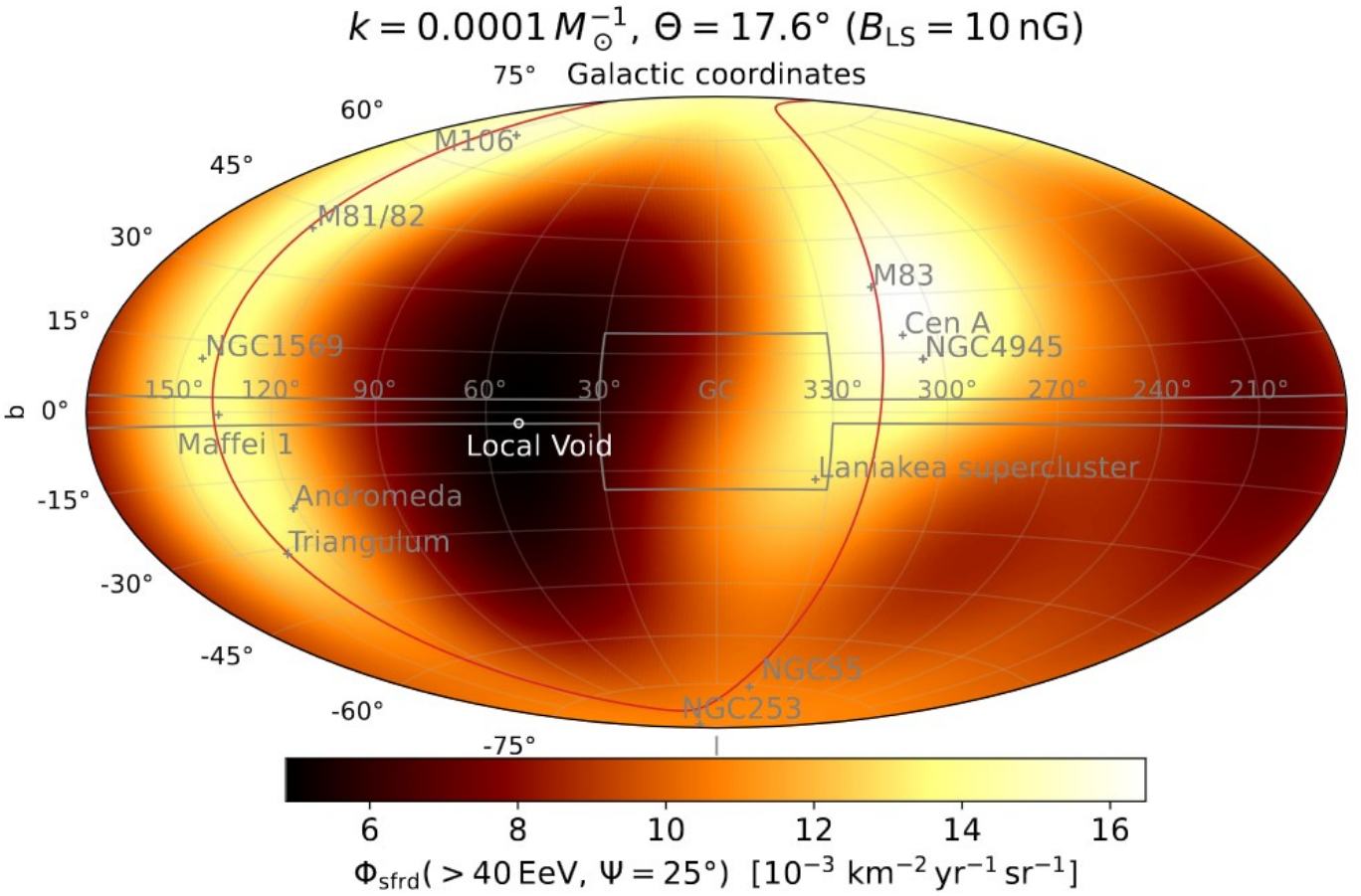

Figure 5. Model flux map of UHECRs at energies above 40 EeV for a burst rate per unit SFR $k = 1 \times 10^{-4}\,M_\odot^{-1}$. The sky map is smoothed using a top-hat function of radius $\Psi = 25\,°$. The red line shows the supergalactic plane. The area delimited by the grey line represents the zone of avoidance. Following Biteau (2021), prominent galaxies and structures contributing to the flux are represented by grey markers and the center of the Local Void is indicated by a white circle. The complete figure set (7 images) is available in Appendix B.

Marafico et al. (2024), to be published in ApJ

What about non-identical sources?

Variation of the maximum rigidity

TABLE III. Best-fit parameters for several variations of the source model. From left to right: the base scenario with SIBYLL2.3c as air shower model and no shifts of the energy- and $X_{\max}$-scales of the data; our fiducial model, SIBYLL2.3c and the $\langle X_{\max}\rangle$ / $\sigma(X_{\max})$ data points shifted by $-1/+1\,\sigma_{\rm syst}$ respectively; the same scale shifts but with EPOS-LHC as air shower model. The injection fractions are given in descending order for p, He, N, Si and Fe. An asterisk indicates that the confidence interval extends to the edge of the scan range and the parameter is not properly constrained in that direction.

Model	SIBYLL2.3c (no shifts)	SIBYLL2.3c (fid. shifts)	EPOS-LHC (fid. shifts)
R_0 [EV]	$1.73^{+0.20}_{-0.18}$	$0.57^{+1.88}_{-0.11}$	$1.6^{+0.6}_{-0.4}$
$\beta_{\rm pop}$	$29.9^{+1.7*}_{-18.1}$	$5.2^{+26.4*}_{-0.5}$	$4.4^{+0.5}_{-0.5}$
$\gamma_{\rm src}$	$-0.23^{+0.18}_{-0.26}$	$-0.8^{+1.4}_{-0.5}$	$0.1^{+0.4}_{-0.5}$
f_A^R[%]	0^{+0}_{-0}	$0^{+36.4}_{-0}$	0^{+0}_{-0}
	$58.1^{+0.4}_{-1.9}$	$0^{+51.3}_{-0}$	$36.9^{+7.4}_{-22.8}$
	$35.0^{+1.6}_{-0.2}$	$93.7^{+0.5}_{-53.5}$	$50.3^{+16.3}_{-5.4}$
	$5.7^{+0.5}_{-0.6}$	$0.3^{+7.7}_{-0.3}$	$11.3^{+6.6}_{-3.8}$
	$1.16^{+0.12}_{-0.11}$	$6.0^{+0.2}_{-3.8}$	$1.41^{+0.27}_{-0.04}$
$R^{0.90}_{\rm max}$ [R_0]	$1.083^{+0.155}_{-0.005}$	$1.72^{+0.13}_{-0.64}$	$1.97^{+0.22}_{-0.17}$
χ^2/d.o.f.	45.0/26	40.4/26	56.3/26

$$\phi_{\rm src}^{\text{b-exp}} = \phi_0\, R^{-\gamma_{\rm src}} \begin{cases} 1 & R < R_{\rm max} \\ \exp\left(1 - \frac{R}{R_{\rm max}}\right) & \text{otherwise,} \end{cases} \quad (5)$$

$$*$$

$$p(R_{\rm max}) = \begin{cases} 0 & R_{\rm max} < R_0 \\ \frac{\beta_{\rm pop}-1}{R_0}\left(\frac{R_{\rm max}}{R_0}\right)^{-\beta_{\rm pop}} & \text{otherwise,} \end{cases} \quad (7)$$

In summary, we have found that the maximum rigidity distribution of UHECR sources is remarkably narrow, necessitating nearly identical ("standard-candle") sources, or a sharp cutoff in the rigidity distribution of the UHECR source population. In the latter case, the low-rigidity tail exacerbates the need for hard injection spectra that has been exposed by prior studies which performed a combined fit of UHECR observations. Our results place strong constraints on the most plausible astrophysical source classes of UHECRs.

Ehlert, Oikonomou and Unger (2023), Phys. Rev. D 107, 103045

What about non-identical sources?

Variation of the spectral index

Explanation for the observed hardening at ~200 GeV/nucleon (CREAM, PAMELA, ATIC)?

Here we calculate the superposition effect of CR spectra, assuming that CRs are originated from SNR-like sources. The injection spectrum of each source is assumed to be a broken power-law function of rigidity with the break from several to tens of GV. The spectral indices are assumed to be Gaussian distributed around some average values. The normalization of each source is derived assuming a constant total energy of CRs above 1 GeV for all sources. Since the particle spectra inferred from the γ-rays might be different from those leaking into the interstellar space [22], the injection parameters are adopted through the fit to the CR data instead of the ones inferred from γ-ray observations.

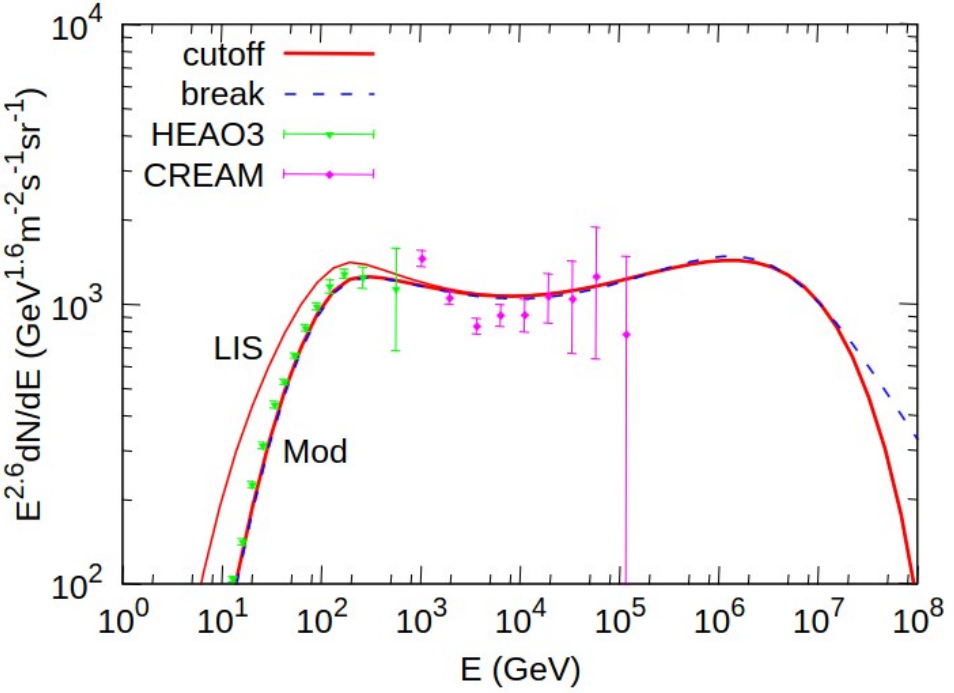

Yuan, Zhang and Bi (2011), Phys. Rev. D 84, 043002

Combined fit ∗ Convolution

Tables of the convoluted equations **implemented in the code of the MICRO combined fit**

	Marafico et al.	γ conv.	$\lg R_{\max}$ conv.	γ+$\lg R_{\max}$ conv.
$\lg(R_{\max}/V)$	18.38±0.04	18.06±0.02	18.22±0.03	18.10±0.01
γ_A	-0.36±0.21	-2.14±0.18	-0.8±0.19	-1.78±0.11
γ_p	2.6±0.7	3.84±0.09	2.78±1.12	3.50±1.18
$k\varepsilon_{\rm tot} \times 10^{46}\,{\rm erg}\,M_\odot^{-1}$	4.8±0.2	5.24±0.19	4.77±0.35	5.16±0.47
f_H / %	19±4	27.9±4.4	18.1±5.7	27.6±7.5
f_{He} / %	14±3	4.7±2.6	14.3±3.5	4.3±2.4
f_{CNO} / %	48±4	52.2±3.8	50.3±4	52.4±2.4
f_{Si} / %	15±3	12.3±3.2	13.7±3.3	12.7±3.4
f_{Fe} / %	4±1	2.9±1.1	3.6±1.3	3.0±1.1
δ_X	1.20±0.18	1.3±0.11	1.09±0.17	1.34±0.15
$D_J + D_X$	22.2+32.1	20.3+22.7	21.3+33.3	19.72+23.62
σ_γ	-	1.56±0.21	-	1.40±0.01
$\sigma_{R_{\max}}$	-	-	0.07±0.03	0±0

Marafico et al. (2024), to be published in ApJ

Standard combined fit

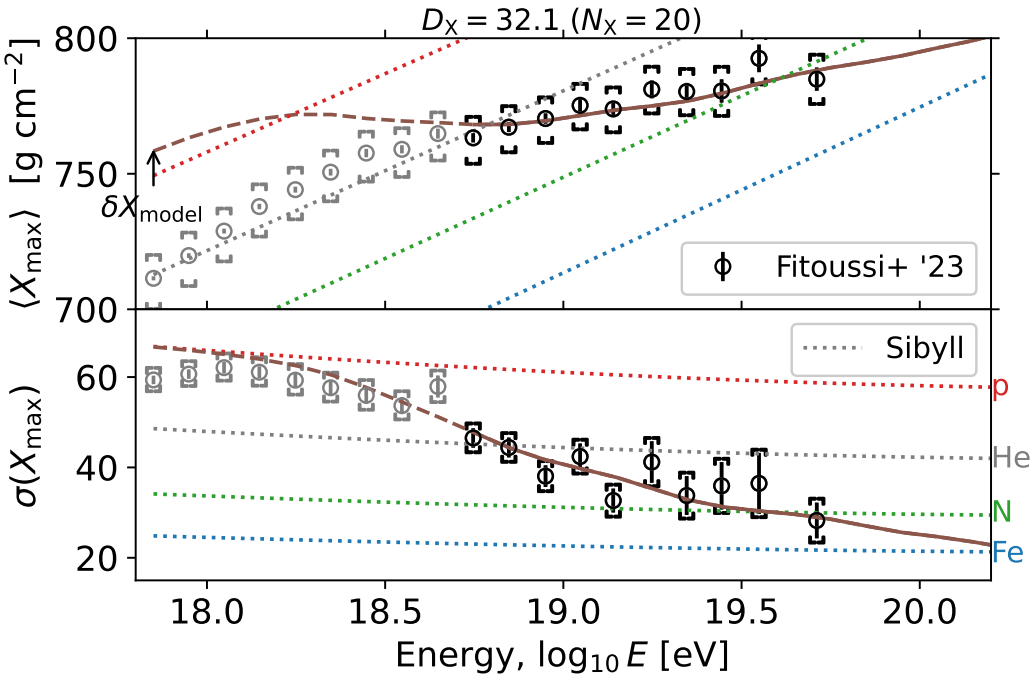

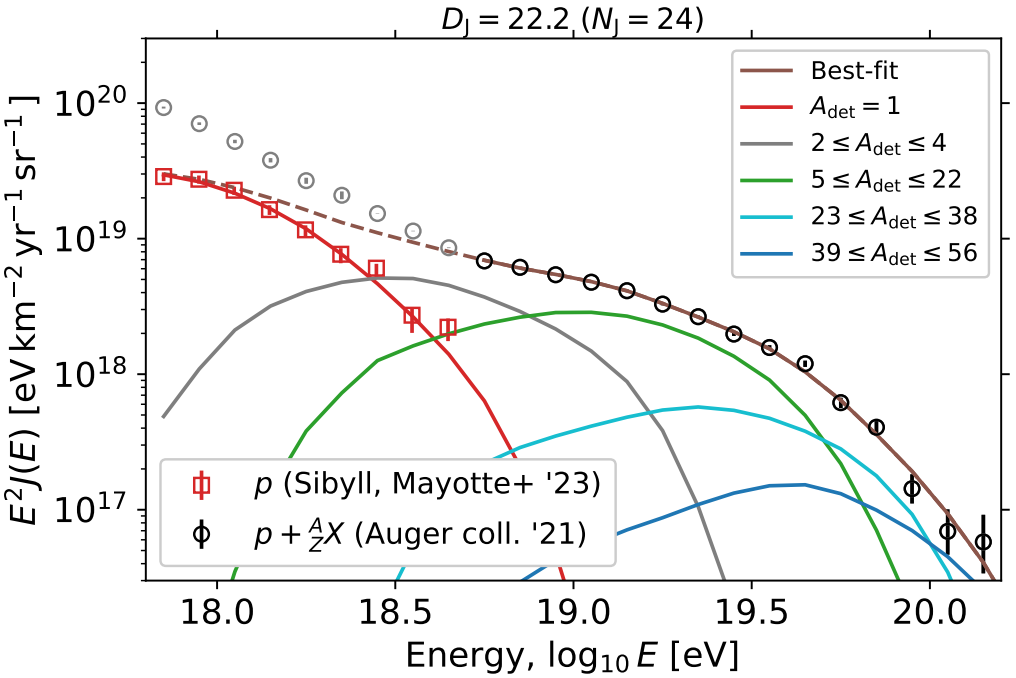

Marafico et al. (2024), to be published in ApJ

Combined fit ∗ γ convolution

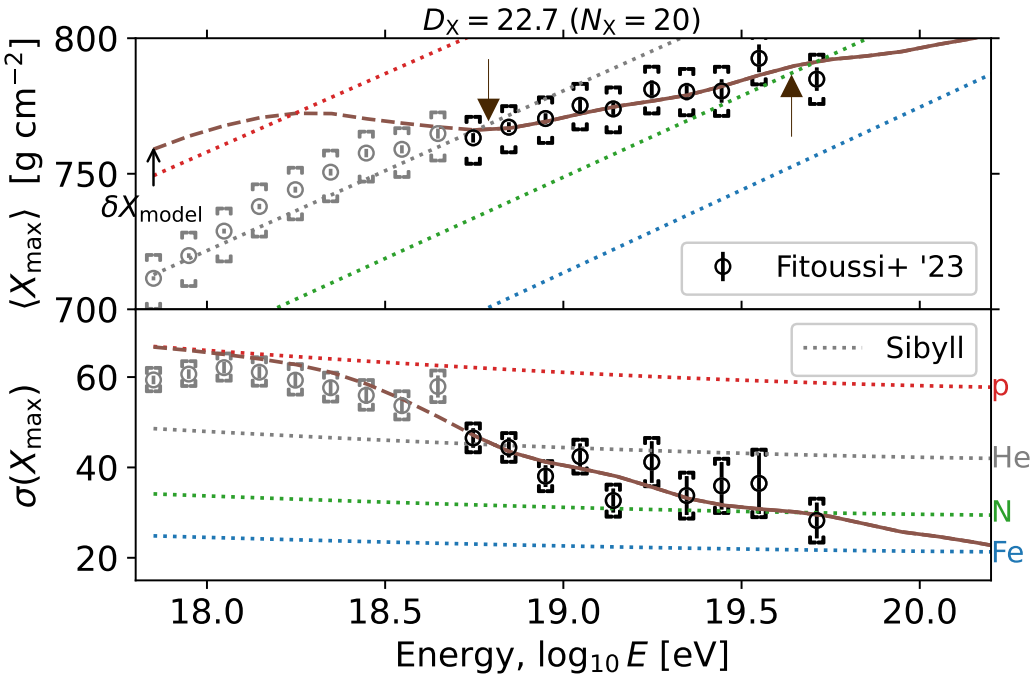

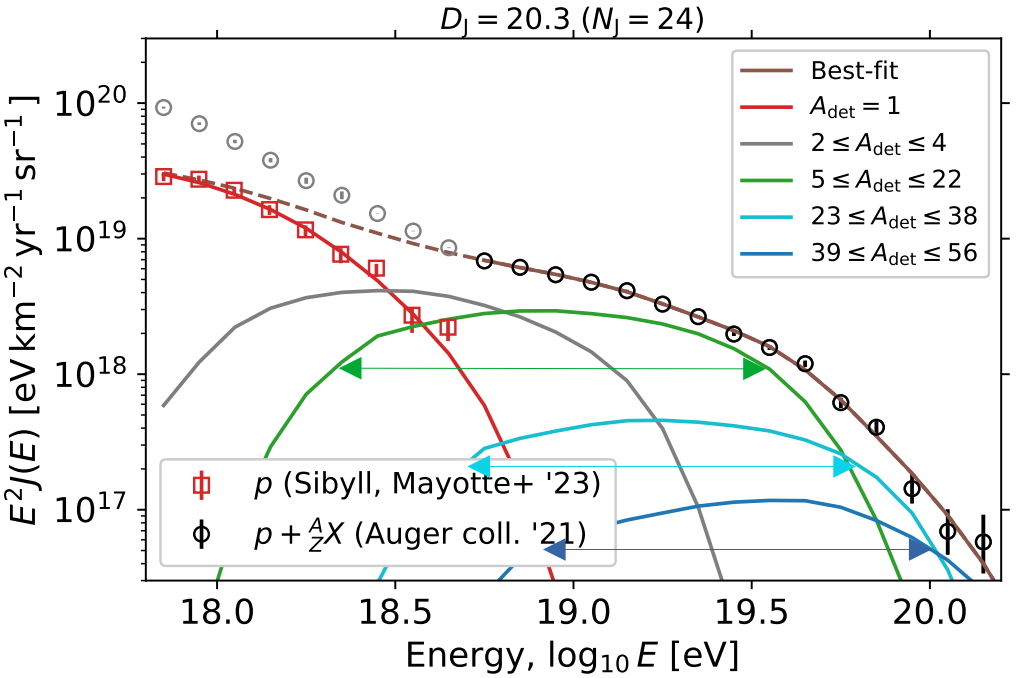

« Contamination » of larger mass number at the intermediate energies, more intermediate masses at the highest energies + **shift of X_{max} towards higher values**

→ **deviance improved by ~11 points**

Combined fit ∗ γ+lg$R_{\max}$ convolution

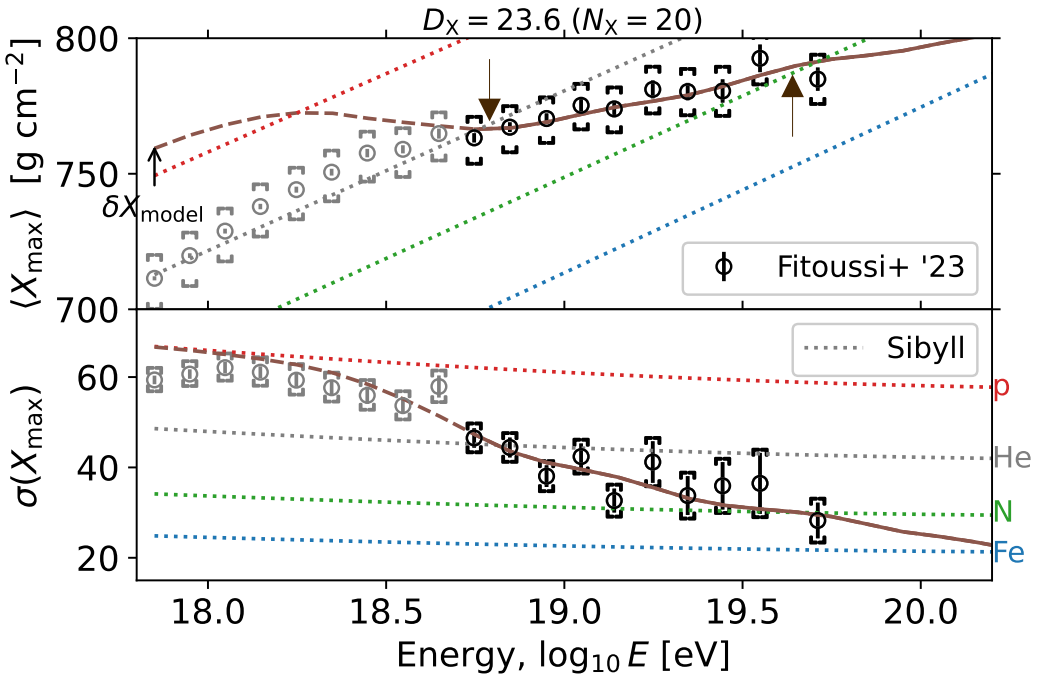

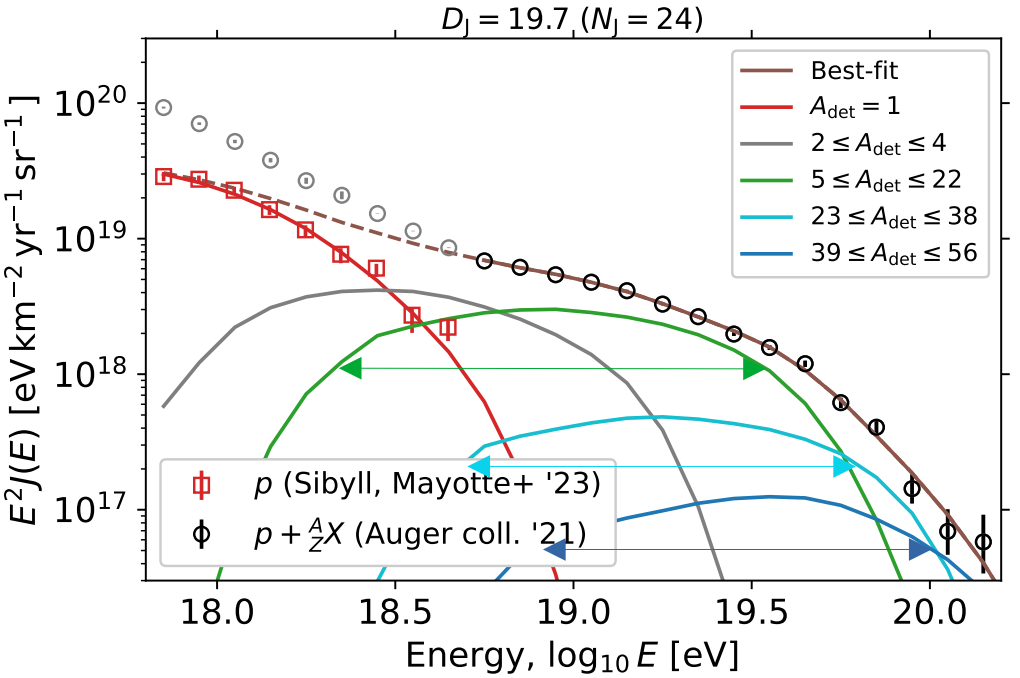

Convolution: What is happening?

$\lg R_{\max} = 18.06$

Why a preference for a large dispersion of spectral index?

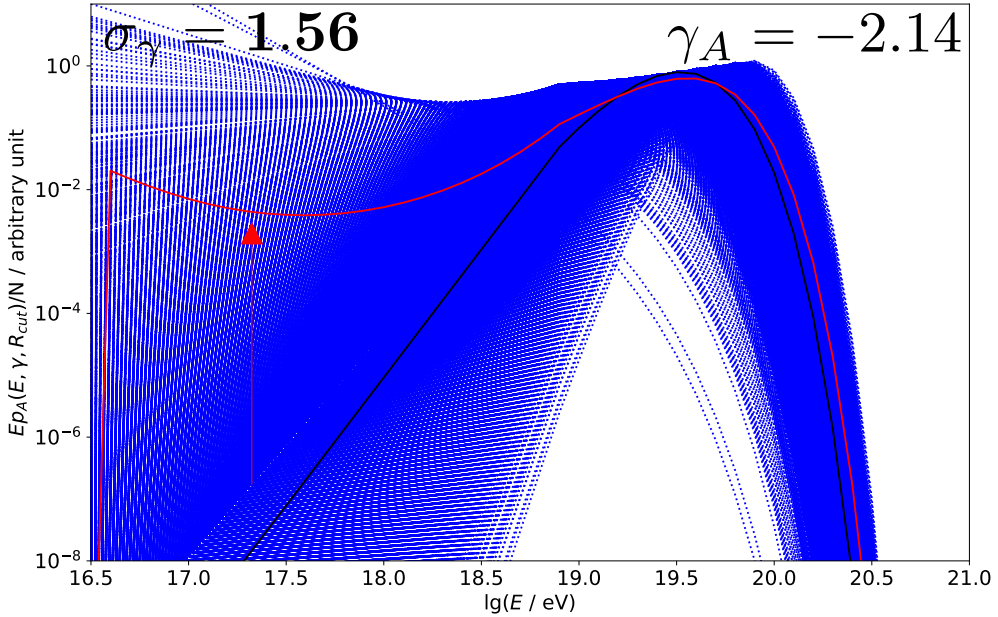

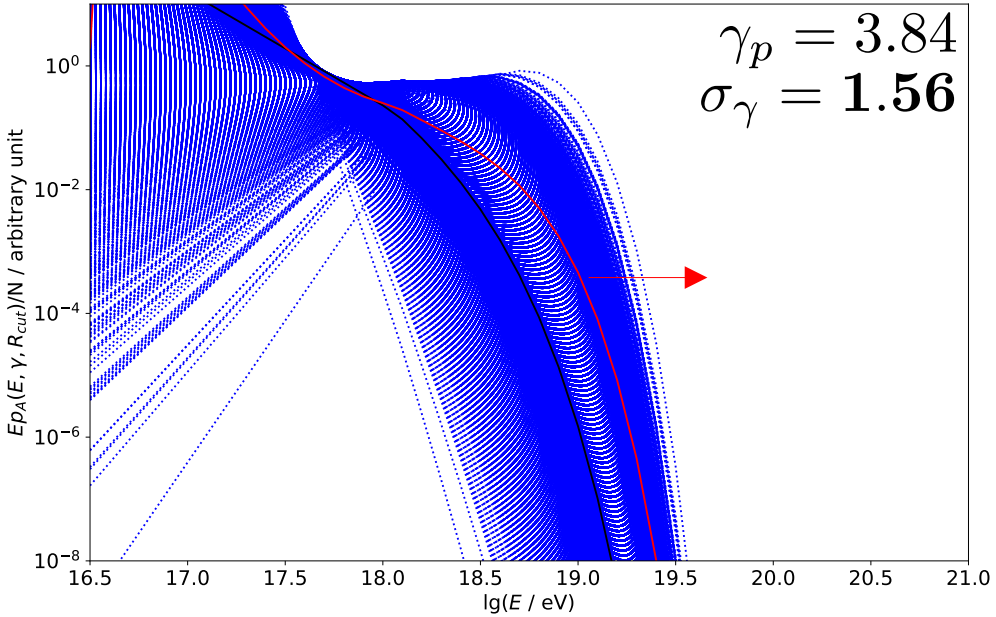

Why a preference for low dispersion of maximal rigidity?

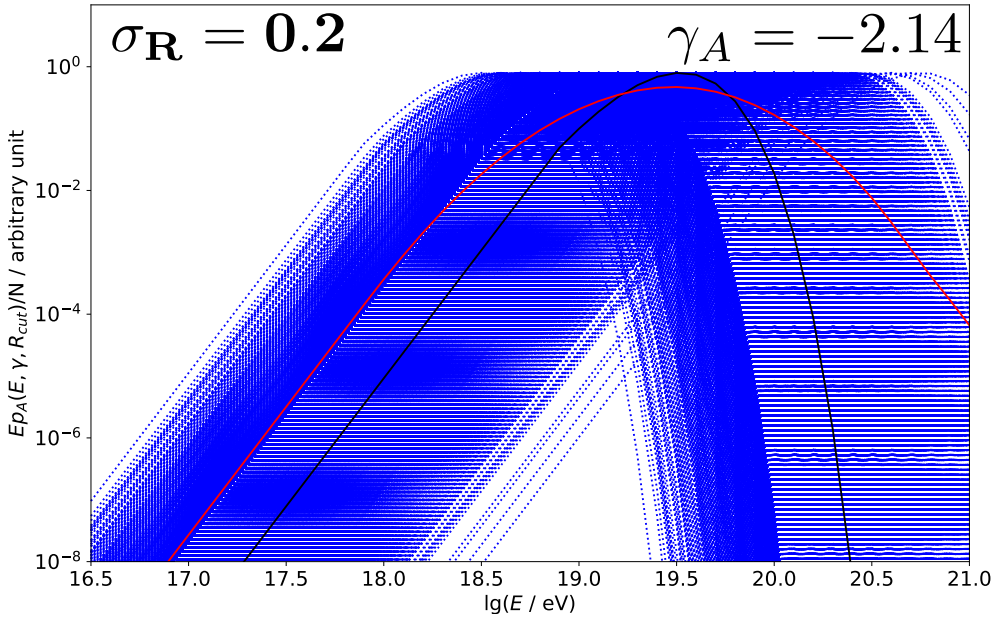

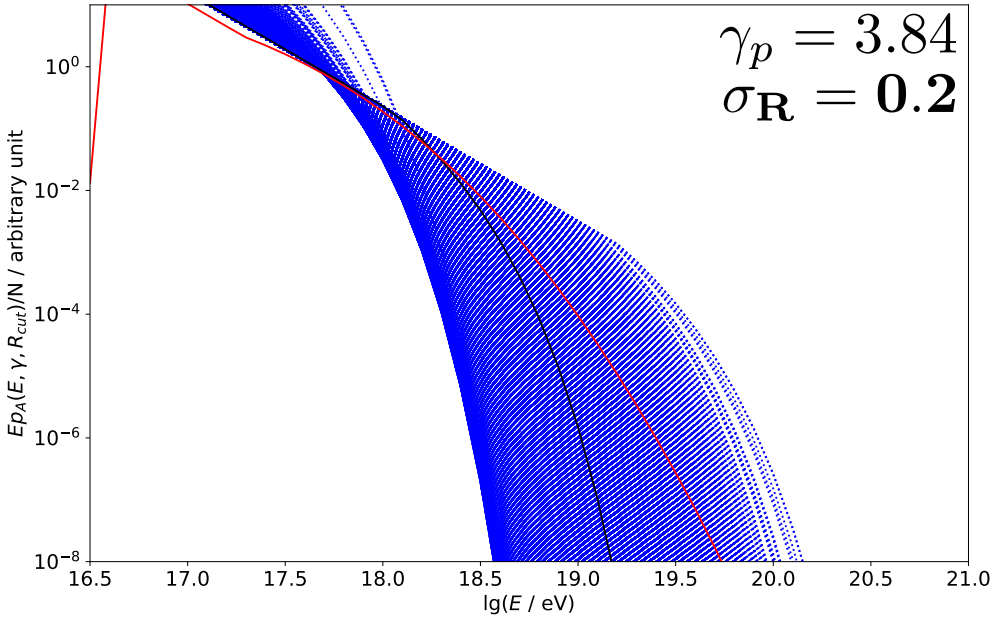

Parameters uncertainties - γ convolution

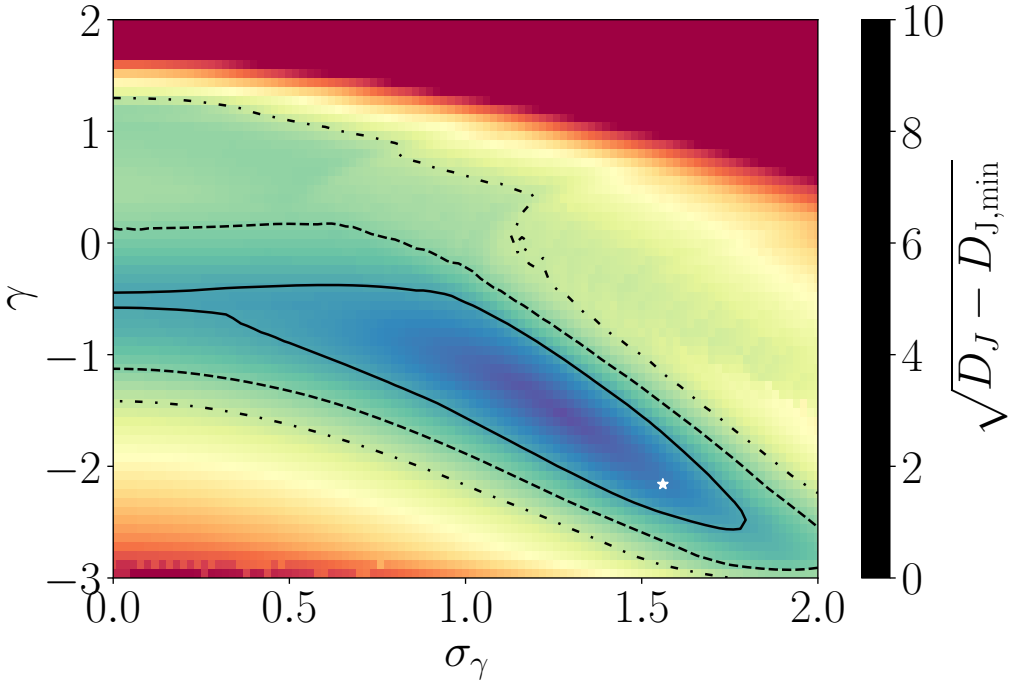

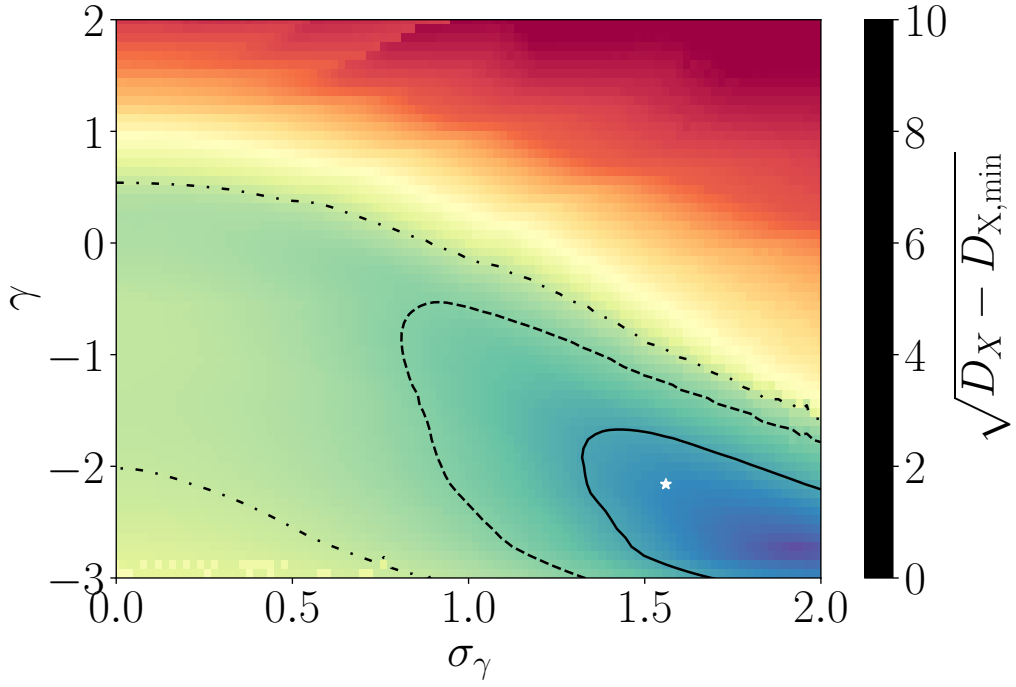

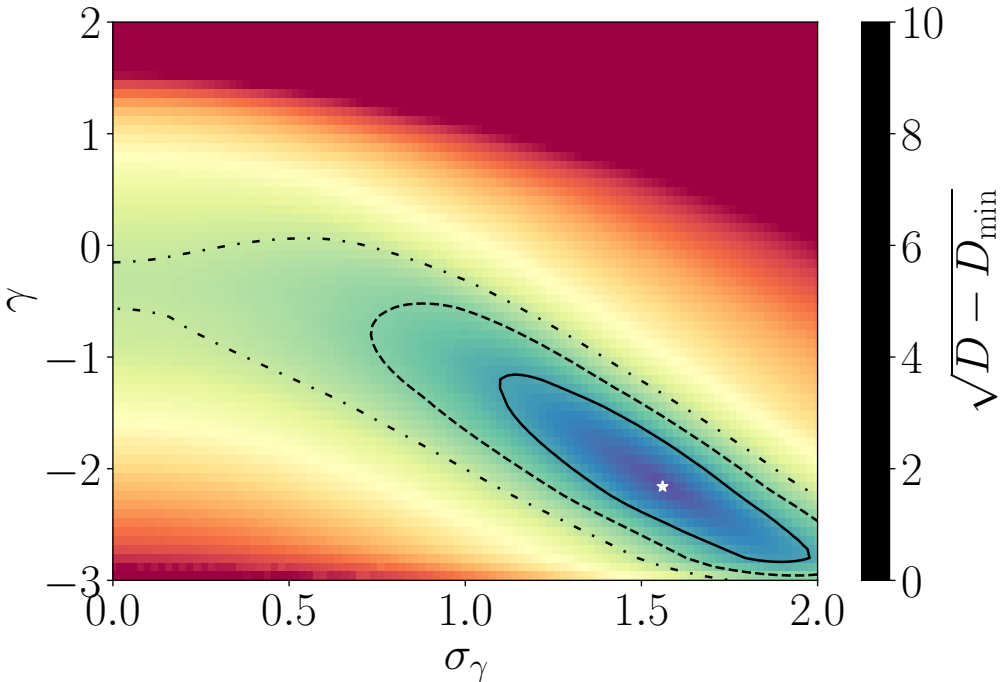

1σ contour
2σ contour
3σ contour

Parameters uncertainties - $\lg R_{\max}$ convolution

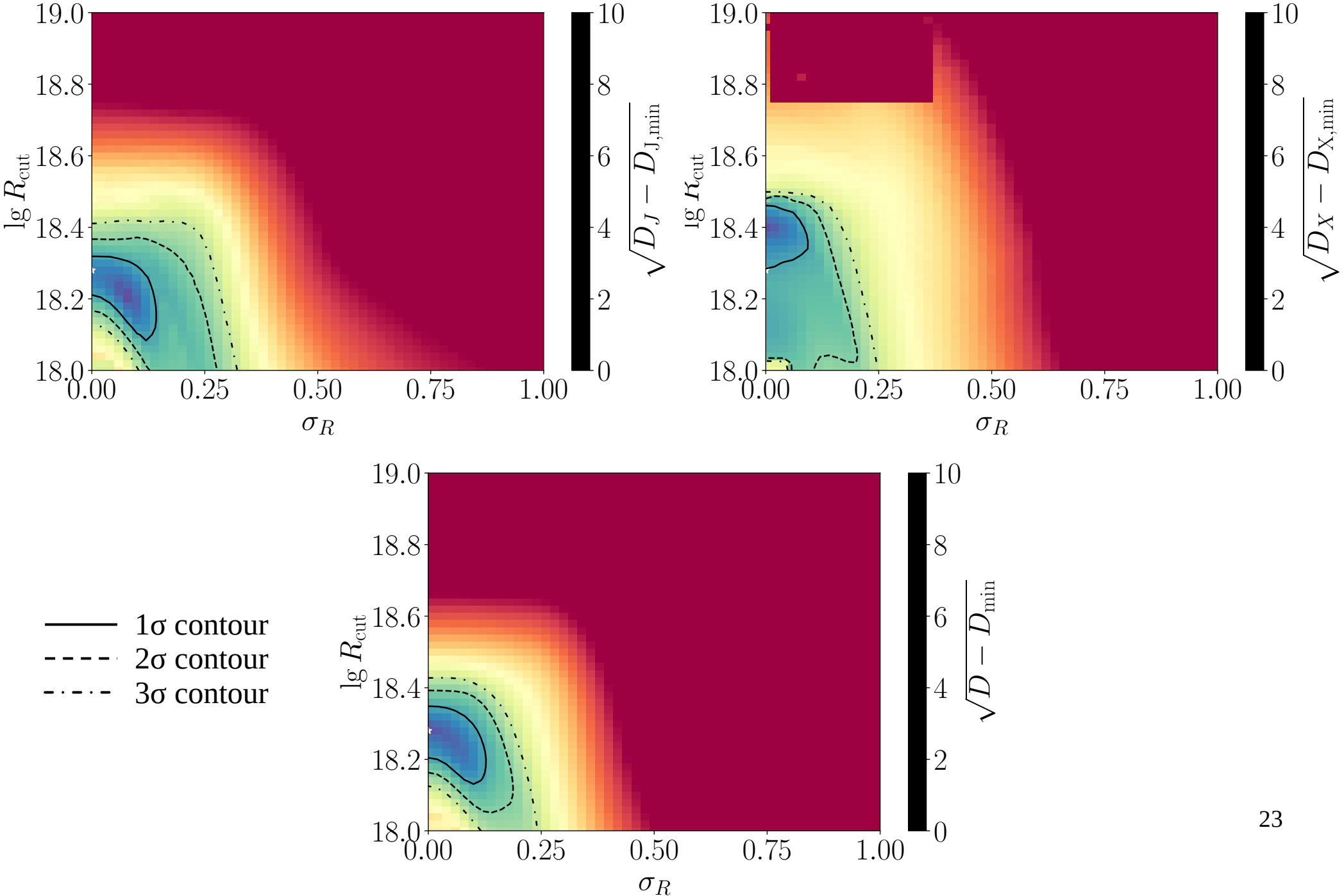

Parameters uncertainties - γ+lgR_{max} convolution

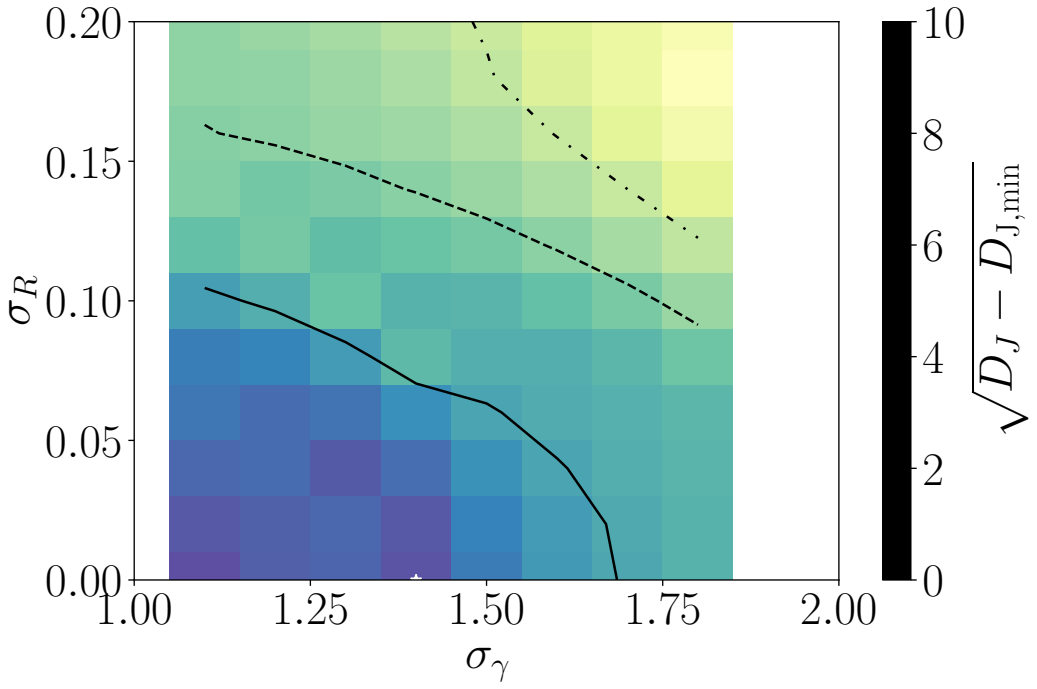

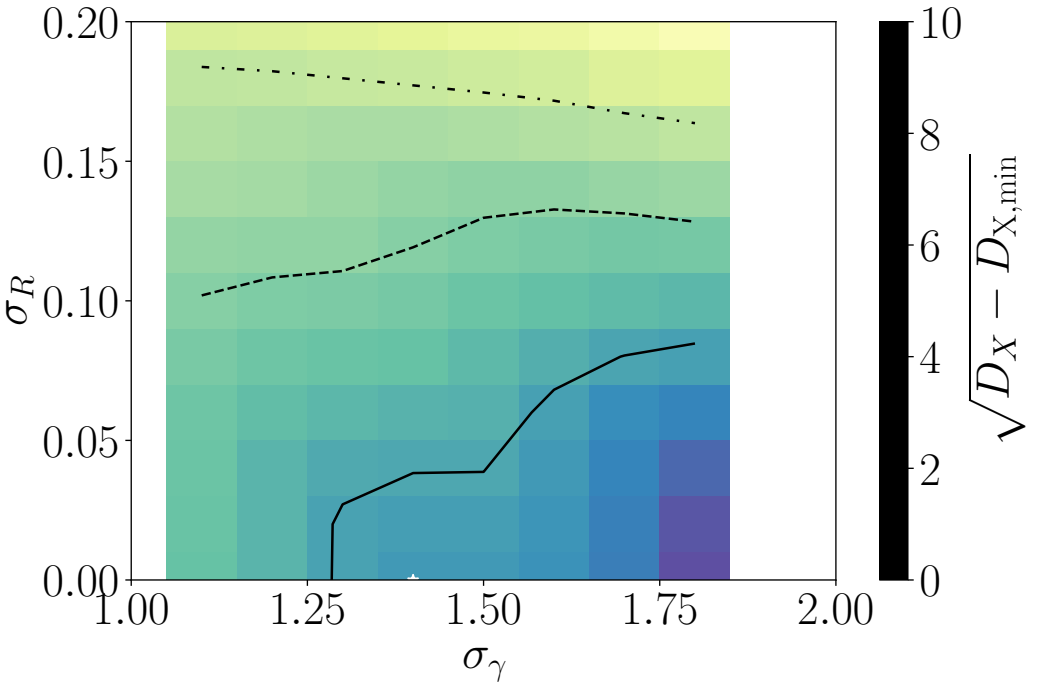

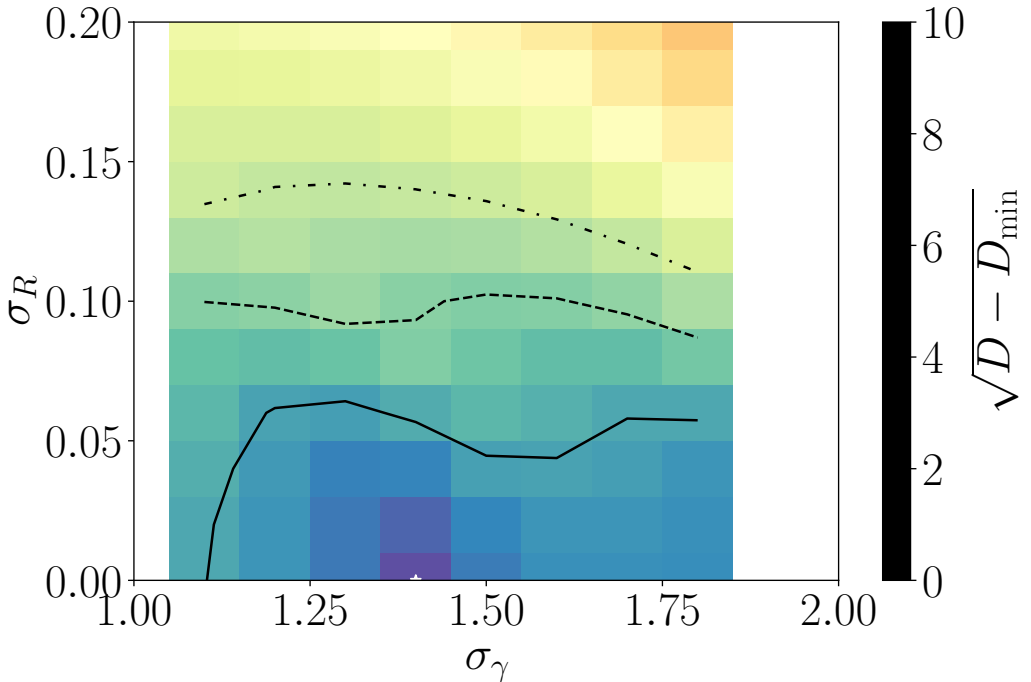

1σ contour
2σ contour
3σ contour

Conclusion

Degeneracy of the parameters of the spectrum when adding a variety of injected spectra?
→ convoluted spectrum = low-energy component + standard power-law spectrum
→ strong correlation between γ and σ_γ
→ 'mass' and 'spectrum' measurements exhibits opposite behaviour

Lower-energy component cannot explain the observations below the ankle
→ mostly secondary protons while 'Hillas B component' would be dominated by CNO

Questions unsolved:
→ choice of the injected masses: Helium?
→ higher masses than iron?
→ dependency with the redshift?

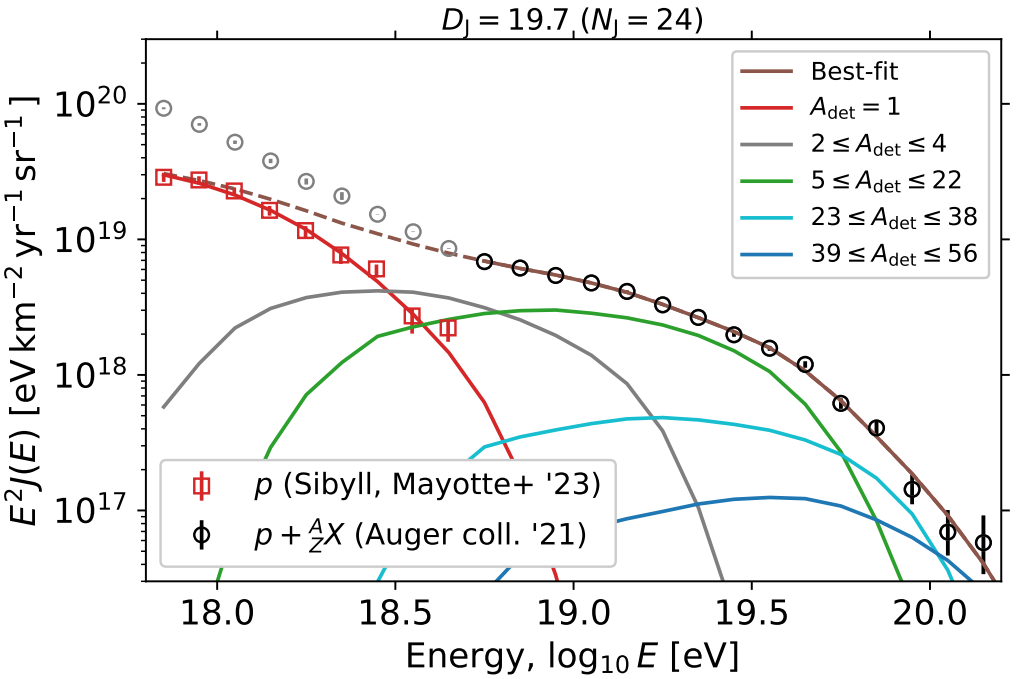

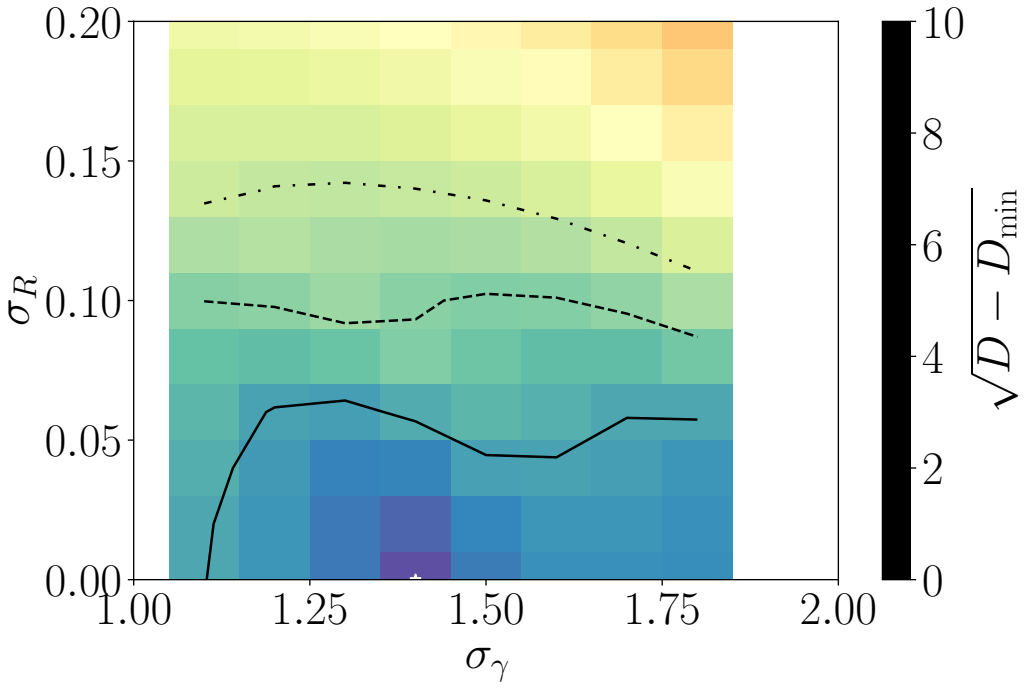

Trugarez !*

* Thank you!

Back-up

Non-identical injection spectrum at the source

How to deal with a variety of galaxies considering:

$$p_A(R,\gamma,R_{\max}) = \frac{Rj(R,\gamma,R_{\max})}{Z\int_{R_{\min}}^{\infty} Rj(R,\gamma,R_{\max})\mathrm{d}R}$$

A Gaussian distribution of the spectral index?

$$p_\gamma(R,\gamma,R_{\max}) = p_A(R,\gamma,R_{\max}) * \mathcal{N}(0,\sigma_\gamma)$$

$$= \frac{f_{\mathrm{supp}}(R,R_{\max})}{\sqrt{2\pi}\sigma_\gamma Z}\int_{-\infty}^{\infty} \frac{R^{1-t}\exp\left(-\frac{1}{2}\left(\frac{\gamma-t}{\sigma_\gamma}\right)^2\right)}{R_{\max}^{2-t}\left(\frac{1}{2-t}+e\Gamma(2-t,1)\right)-\frac{R_{\min}^{2-t}}{2-t}}\,\mathrm{d}t$$

A Gaussian distribution of the logarithm of the maximum rigidity?

$$p_{R_{\max}}(R,\gamma,R_{\max}) = p_A(R,\gamma,R_{\max}) * \mathcal{N}(0,\sigma_R)$$

$$= \frac{R^{1-\gamma}}{\sqrt{2\pi}\sigma_R Z}\begin{cases} \int_{-\infty}^{\infty} \frac{\exp\left(-\frac{1}{2}\left(\frac{\lg R_{\max}-r}{\sigma_R}\right)^2\right)}{10^{(2-\gamma)r}\left(\frac{1}{2-\gamma}+e\Gamma(2-\gamma,1)\right)-\frac{R_{\min}^{2-\gamma}}{2-\gamma}}\mathrm{d}r & \text{if } R < R_{\max}, \\ \int_{-\infty}^{\infty} \frac{\exp\left(1-\frac{R}{10^r}-\frac{1}{2}\left(\frac{\lg R_{\max}-r}{\sigma_R}\right)^2\right)}{10^{(2-\gamma)r}\left(\frac{1}{2-\gamma}+e\Gamma(2-\gamma,1)\right)-\frac{R_{\min}^{2-\gamma}}{2-\gamma}}\mathrm{d}r & \text{otherwise.} \end{cases}$$

An extension of CNO-like

Test of a different shape to describe the end of the injected spectra:

$$\mathrm{j(R},\,\gamma, R_{\max}) \propto \left(\frac{R}{R_0}\right)^{-\gamma} \mathrm{sech}\left(\left(\frac{R}{R_{\max}}\right)^{\Delta}\right)$$

	Marafico et al.	γ conv.	$\Delta = 2$	$\Delta = 2,\ \delta X = 0$
$\lg(R_{\max}/V)$	18.38±0.04	18.06±0.02	18.80±0.01	18.79±0.01
γ_A	-0.36±0.21	-2.14±0.18	0.73±0.04	0.5±0.03
γ_p	2.6±0.7	3.84±0.9	3.85±0.47	4±0
$k\varepsilon_{\mathrm{tot}} \times 10^{46}\,\mathrm{erg}\,M_{\odot}^{-1}$	4.8±0.2	5.24±0.19	5.63±0.46	5.14±0.23
f_H	19±4	27.9±4.4	32.8±7.7	19.6±4.6
f_{He}	14±3	4.7±2.6	0±0	4.3±1.7
f_{CNO}	48±4	52.2±3.8	55.5±2.3	66.5±2.9
f_{Si}	15±3	12.3±3.2	8.1±2.4	8.5±2.4
f_{Fe}	4±1	2.9±1.1	3.6±1.0	1.1±0.9
δ_X	1.20±0.18	1.3±0.11	1.41±0.1	-
$D_J + D_X$	22.2+32.1	20.3+22.7	29.2+21.17	69.19+103.16
σ_γ	-	1.56±0.21	-	-

A. Abdul Halim et al.

Marafico et al. (2024), to be published in ApJ
A. Abdul Halim et al. [The Pierre Auger Collaboration] , JCAP 05 (2023) 024

An extension of CNO-like

Test of a different shape to describe the end of the injected spectra:

$$\mathrm{j(R,\,\gamma, R_{max})} \propto \left(\frac{R}{R_0}\right)^{-\gamma} \mathrm{sech}\left(\left(\frac{R}{R_{\mathrm{max}}}\right)^{\Delta}\right)$$

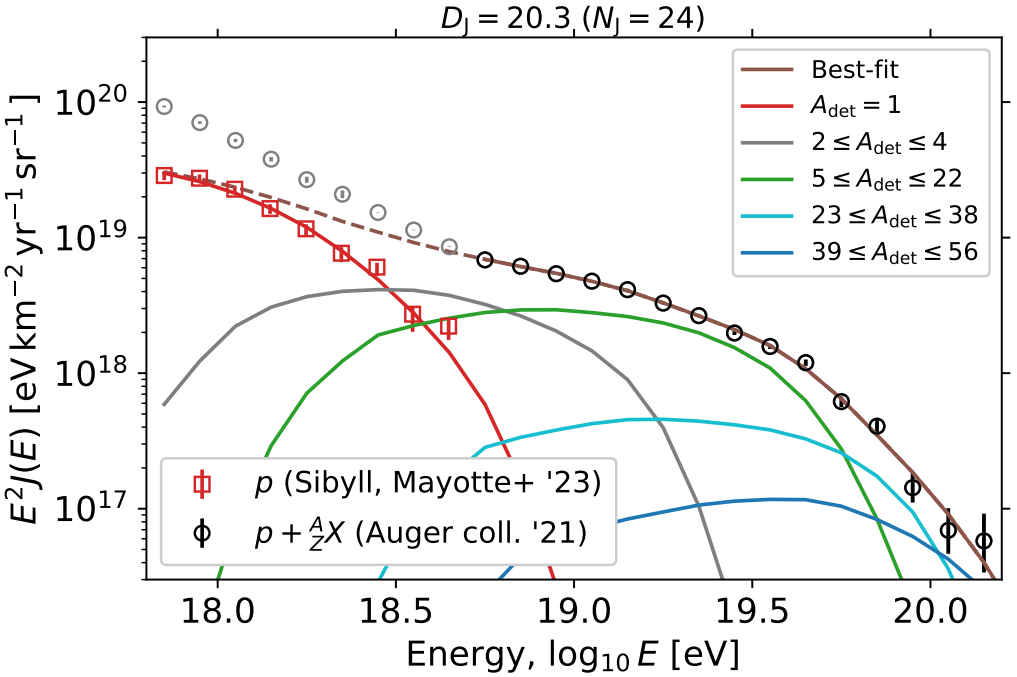

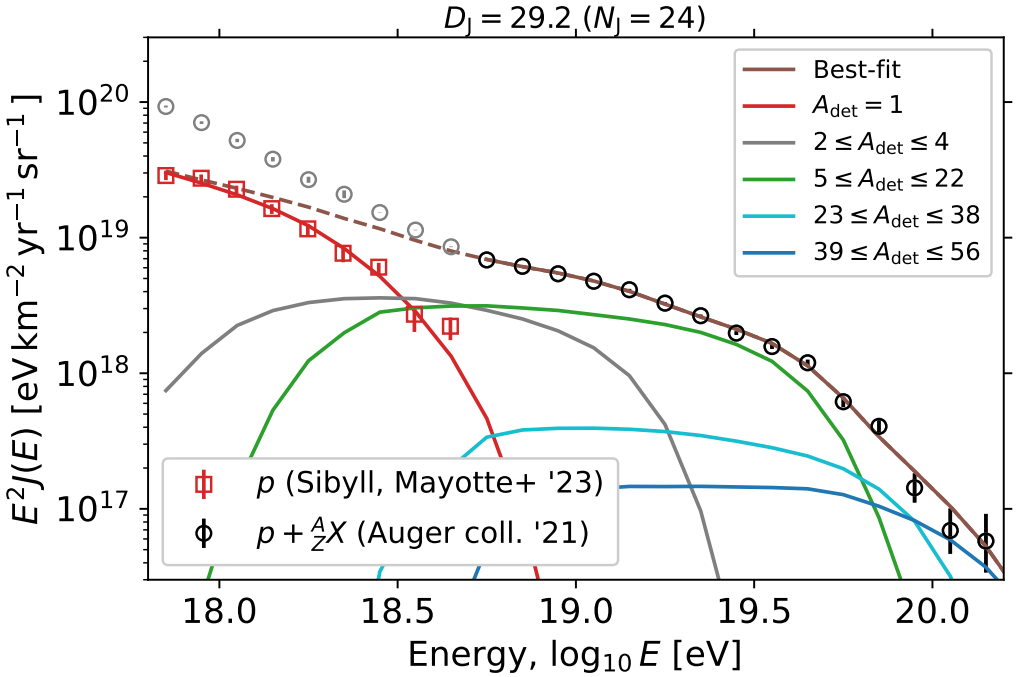

Combined fit ∗ lg$R_{\max}$ convolution

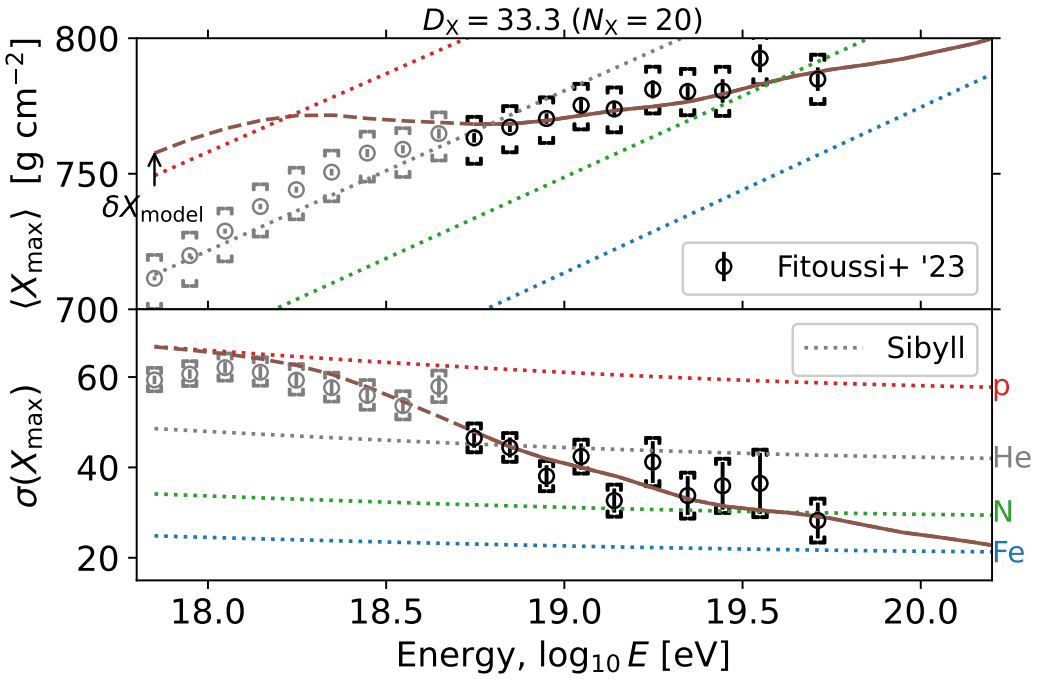

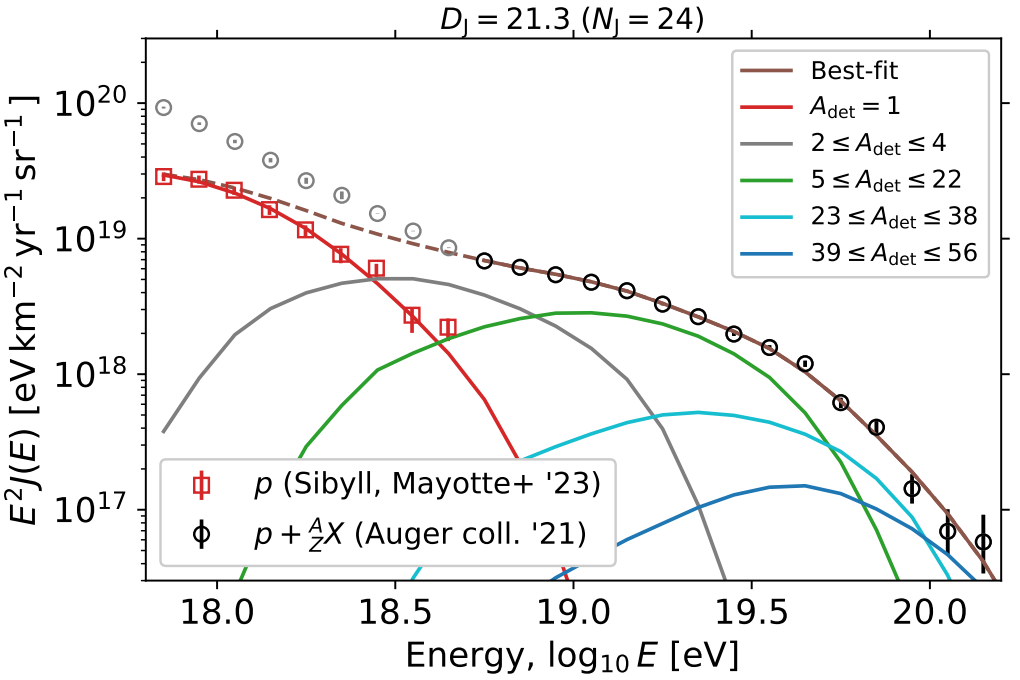

Spectrum normalization

$$\mathrm{N}^{-1} = \int_{E_{\min}}^{\infty} Ej(E,\gamma,R_{\max})\mathrm{d}E = \begin{cases} E_0^2 \left(\ln\left(\frac{E_{\max}}{E_{\min}}\right) + e\Gamma(0,1)\right), \text{if } \gamma = 2 \\ E_0^{\gamma}\left[E_{\max}^{2-\gamma}\left(\frac{1}{2-\gamma} + e\Gamma(2-\gamma,1)\right) - \frac{E_{\min}^{2-\gamma}}{2-\gamma}\right], \text{otherwise} \end{cases}$$

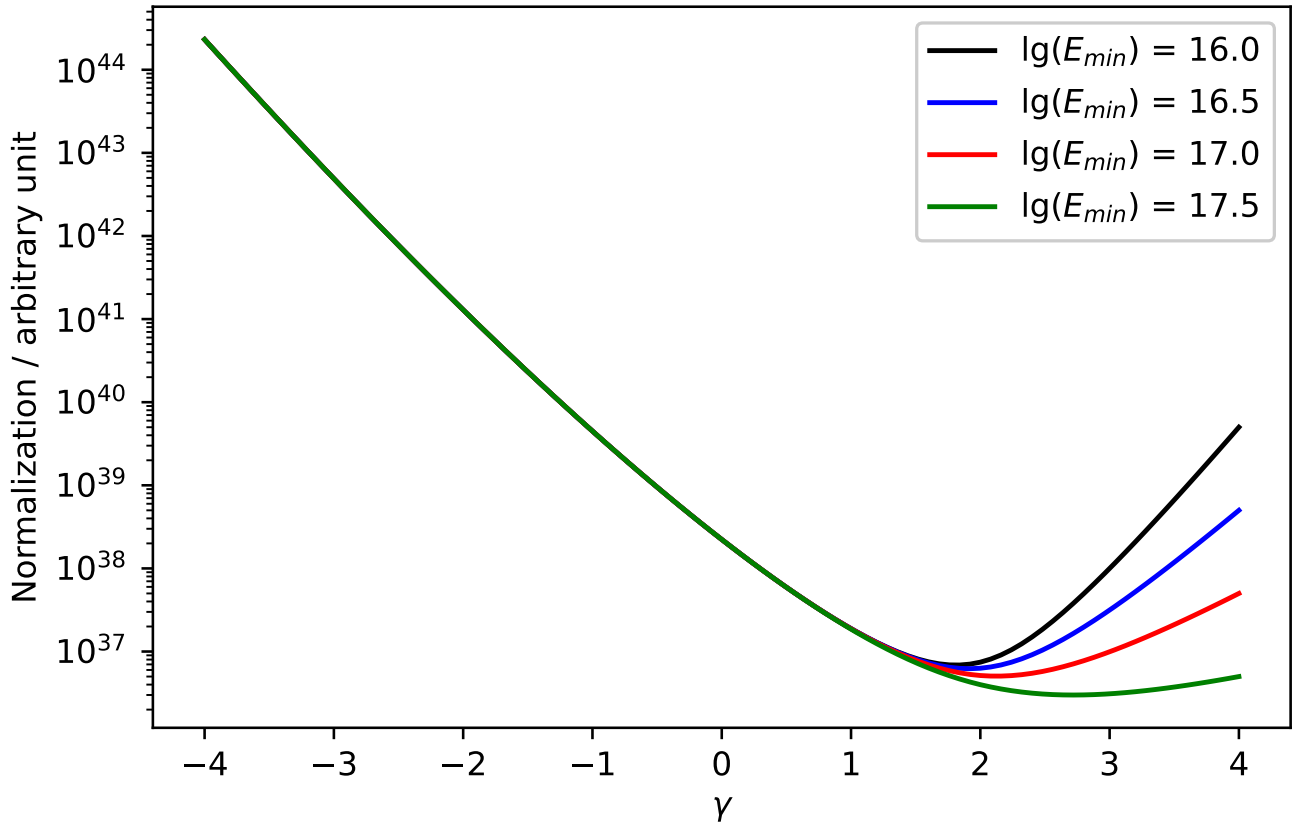

Shape of the end of the spectrum

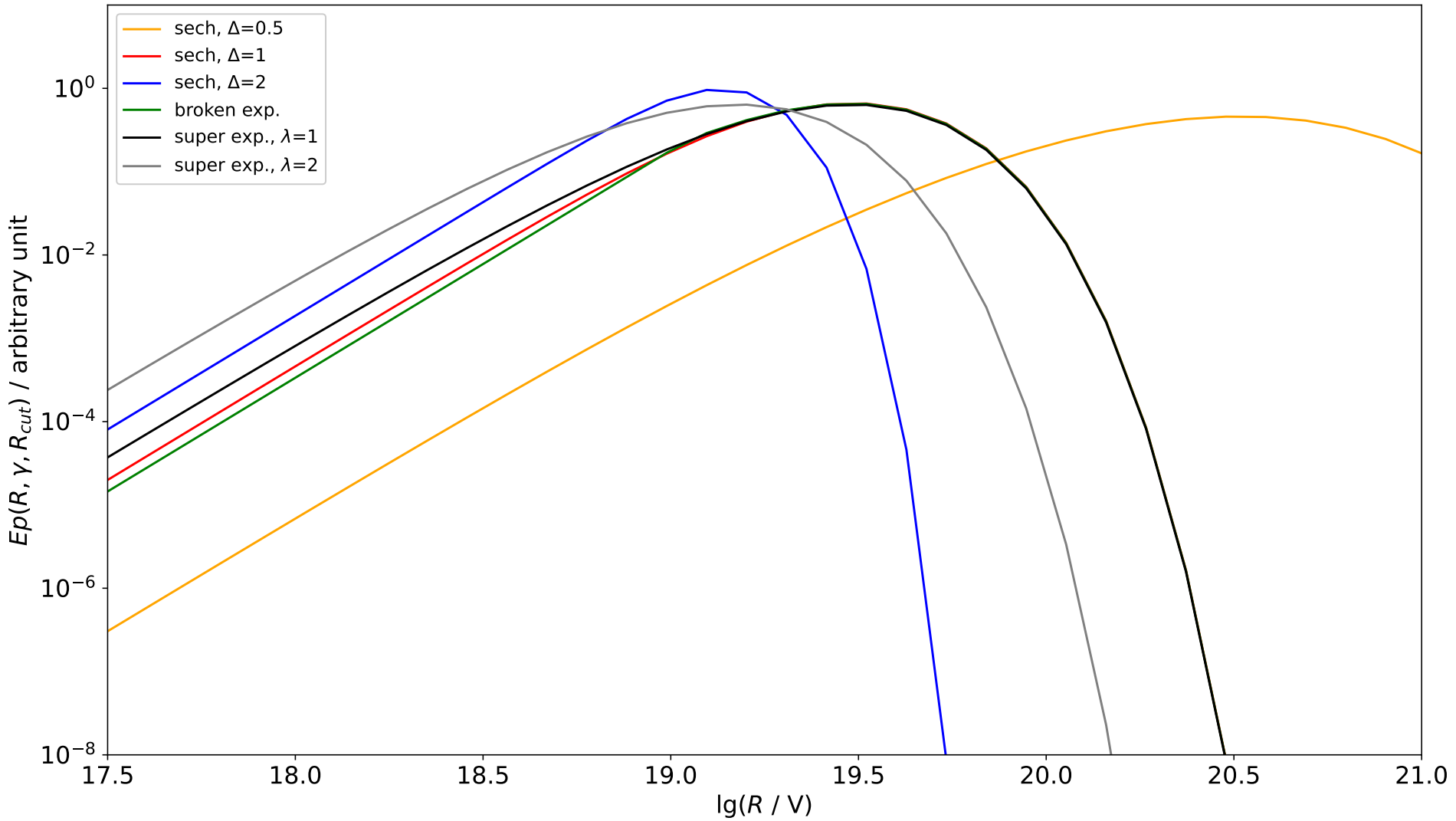

Effective spectral indexes

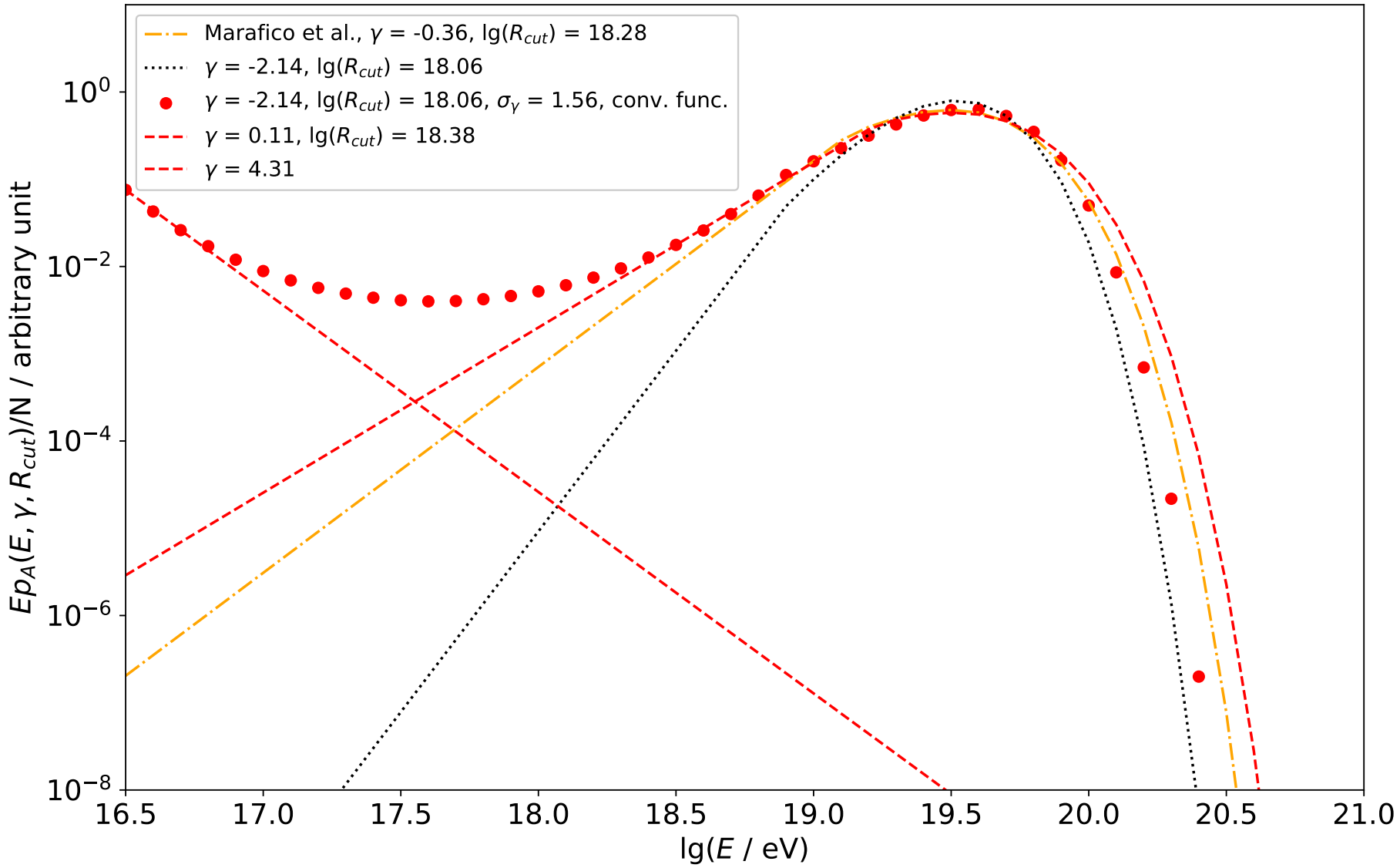

Effective spectral indexes

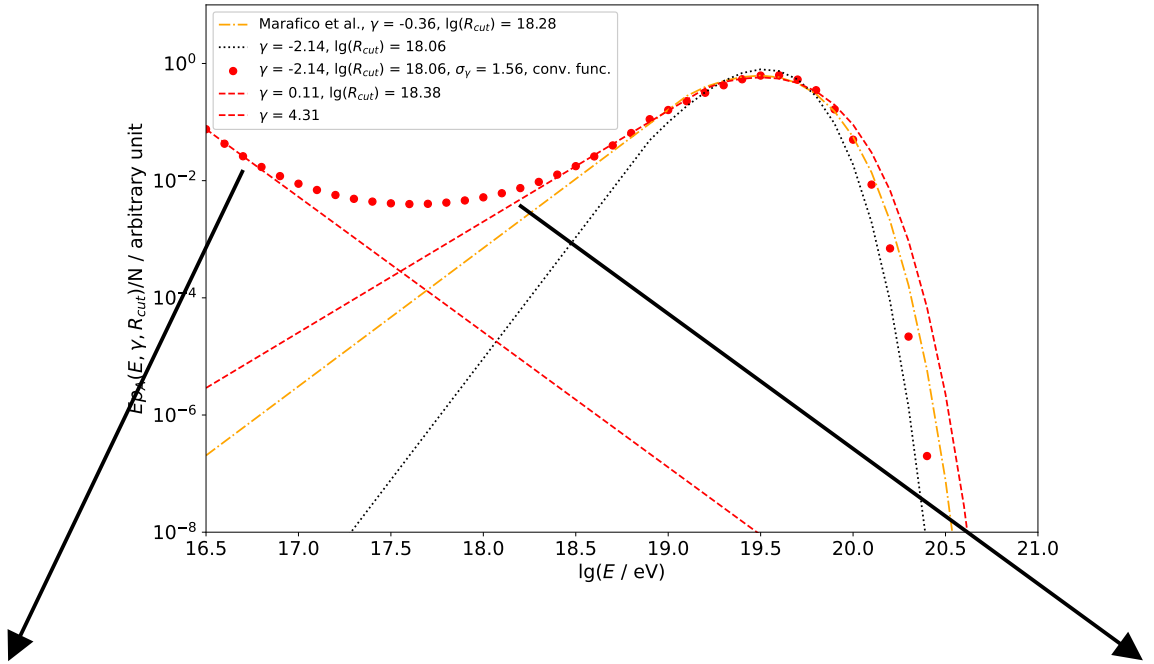

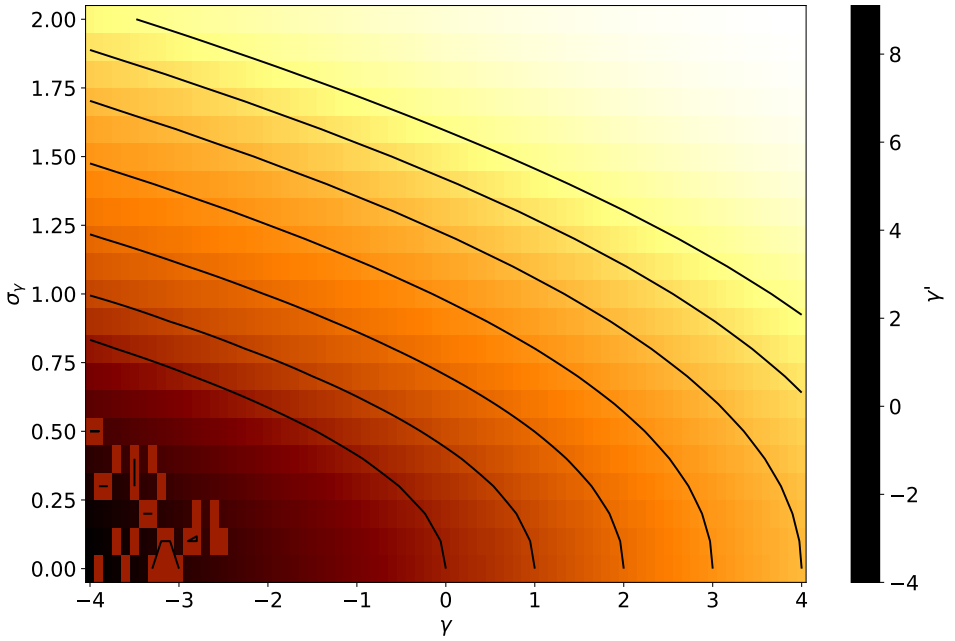

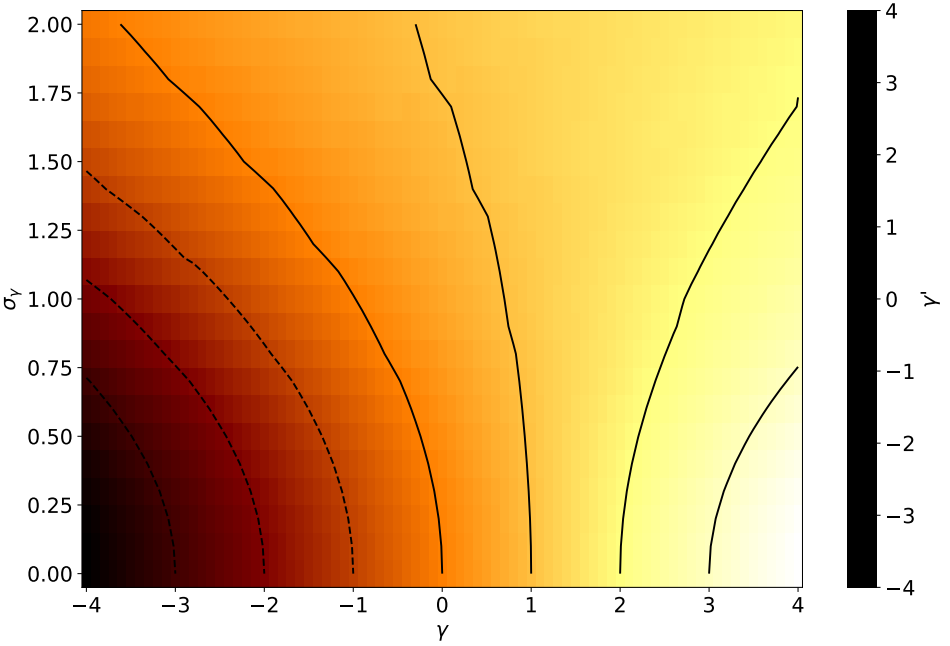

Scan : fraction's results

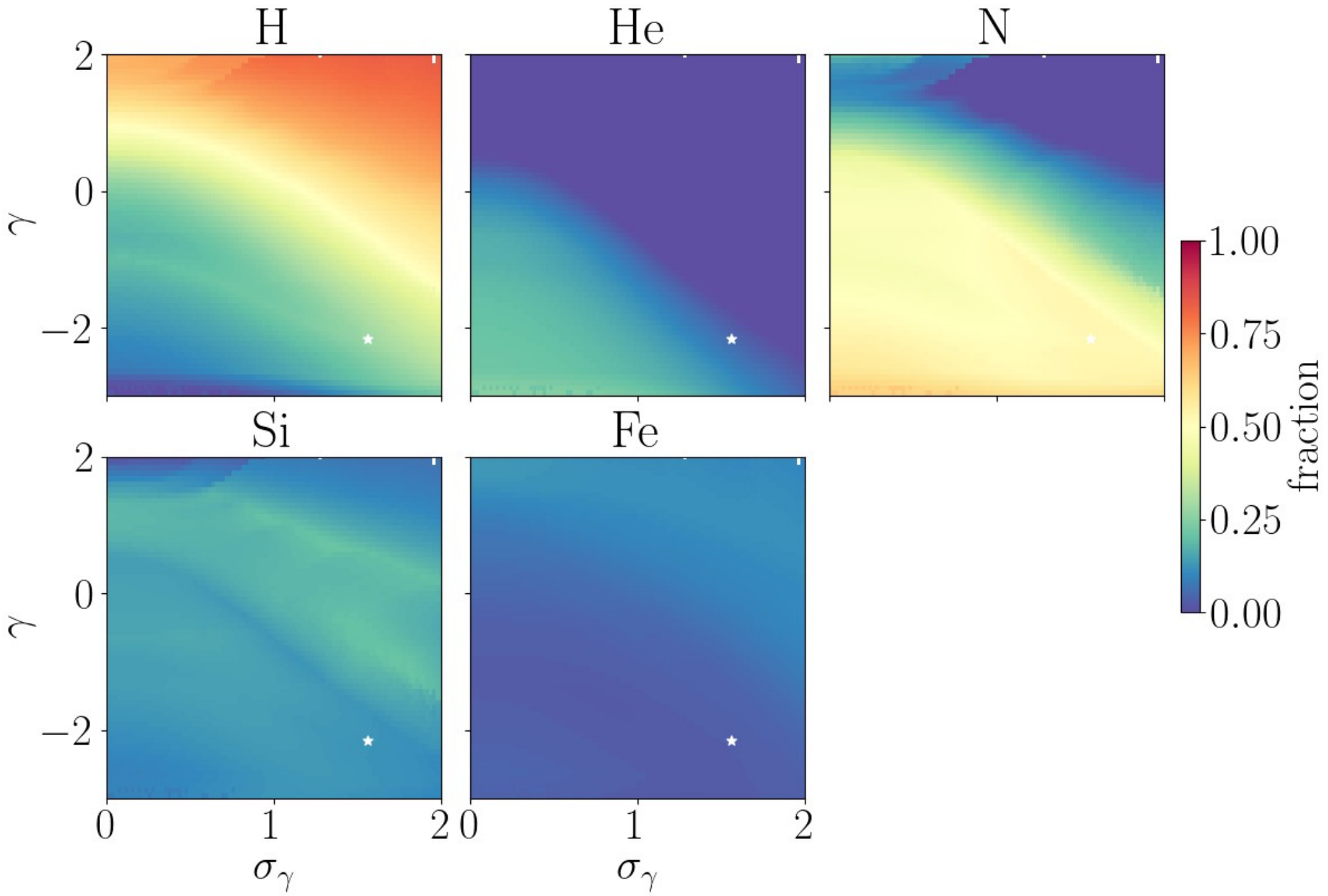

Scan : fraction's results